

# JGR Space Physics

## RESEARCH ARTICLE

10.1029/2020JA028066

### Key Points:

- Slow and fast electron holes are present in the Earth's magnetotail and produced by instabilities operating independently
- The velocity gap in distribution of electron hole velocities is the evidence for self-acceleration or ion Landau damping of electron holes
- The transverse instability and nonlinear saturation criterion of electron streaming instabilities can control electron hole amplitudes

### Supporting Information:

- Supporting Information S1

### Correspondence to:

A. Lotekar,  
ablotekar@gmail.com

### Citation:

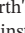







Lotekar, A., Vasko, I. Y., Mozer, F. S., Hutchinson, I., Artemyev, A. V., Bale, S. D., et al. (2020). Multisatellite MMS analysis of electron holes in the Earth's magnetotail: Origin, properties, velocity gap, and transverse instability. *Journal of Geophysical Research: Space Physics*, 125, e2020JA028066. <https://doi.org/10.1029/2020JA028066>

Received 31 MAR 2020

Accepted 10 AUG 2020

Accepted article online 22 AUG 2020

## Multisatellite MMS Analysis of Electron Holes in the Earth's Magnetotail: Origin, Properties, Velocity Gap, and Transverse Instability

A. Lotekar<sup>1</sup> , I. Y. Vasko<sup>2</sup> , F. S. Mozer<sup>2</sup> , I. Hutchinson<sup>3</sup> , A. V. Artemyev<sup>4,5</sup> , S. D. Bale<sup>2</sup> , J. W. Bonnell<sup>2</sup> , R. Ergun<sup>6</sup> , B. Giles<sup>7</sup> , Yu. V. Khotyaintsev<sup>8</sup> , P.-A. Lindqvist<sup>9</sup> , C. T. Russell<sup>5</sup> , and R. Strangeway<sup>5</sup> 

<sup>1</sup>Indian Institute of Geomagnetism, Navi Mumbai, India, <sup>2</sup>Space Sciences Laboratory, University of California, Berkeley, CA, USA, <sup>3</sup>Plasma Science and Fusion Center and Department of Nuclear Science, Massachusetts Institute of Technology, Cambridge, MA, USA, <sup>4</sup>Space Research Institute of Russian Academy of Sciences, Moscow, Russia, <sup>5</sup>Institute of Geophysics and Planetary Sciences, University of California, Los Angeles, CA, USA, <sup>6</sup>Laboratory for Atmospheric and Space Physics, University of Colorado Boulder, Boulder, CO, USA, <sup>7</sup>NASA Goddard Space Flight Center, Greenbelt, MD, USA, <sup>8</sup>Swedish Institute of Space Physics, Uppsala, Sweden, <sup>9</sup>Division of space and plasma physics, KTH Royal Institute of Technology, Stockholm, Sweden

**Abstract** We present a statistical analysis of more than 2,400 electrostatic solitary waves interpreted as electron holes (EH) measured aboard at least three Magnetospheric Multiscale (MMS) spacecraft in the Earth's magnetotail. The velocities of EHs are estimated using the multispacecraft interferometry. The EH velocities in the plasma rest frame are in the range from just a few km/s, which is much smaller than ion thermal velocity  $V_{Ti}$ , up to 20,000 km/s, which is comparable to electron thermal velocity  $V_{Te}$ . We argue that fast EHs with velocities larger than about  $0.1V_{Te}$  are produced by bump-on-tail instabilities, while slow EHs with velocities below about  $0.05V_{Te}$  can be produced by warm bistream and, probably, Buneman-type instabilities. We show that typically fast and slow EHs do not coexist, indicating that the instabilities producing EHs of different types operate independently. We have identified a gap in the distribution of EH velocities between  $V_{Ti}$  and  $2V_{Ti}$ , which is considered to be the evidence for self-acceleration (Zhou & Hutchinson, 2018) or ion Landau damping of EHs. Parallel spatial scales and amplitudes of EHs are typically between  $\lambda_D$  and  $10\lambda_D$  and between  $10^{-3}T_e$  and  $0.1T_e$ , respectively. We show that electrostatic potential amplitudes of EHs are below the threshold of the transverse instability and highly likely restricted by the nonlinear saturation criterion of electron streaming instabilities seeding electron hole formation:  $e\Phi_0 \lesssim m_e \varpi^2 d_{\parallel}^2$ , where  $\varpi = \min(\gamma, 1.5\omega_{ce})$ , where  $\gamma$  is the increment of instabilities seeding EH formation, while  $\omega_{ce}$  is electron cyclotron frequency. The implications of the presented results are discussed.

## 1. Introduction

Electron phase space holes are electrostatic solitary waves with a bipolar parallel electric field produced in a nonlinear stage of various electron streaming instabilities (see, e.g., numerical simulations by Che et al., 2010; Drake et al., 2003; Goldman et al., 1999, 2008; Jara-Almonte et al., 2014; Morse & Nielson, 1969a; Omura et al., 1996; Pommois et al., 2017). These solitary waves are Debye-scale structures with positive electrostatic potentials and exist due to a dearth of the phase space density of electrons trapped by the bipolar parallel electric field (Dupree, 1982; Gurevich, 1968; Krasovsky et al., 1997; Schamel, 1986, 2000). Electrostatic solitary waves interpreted in terms of electron phase space holes were observed in laboratory experiments (Fox et al., 2008; Kovalenko, 1983; Lefebvre et al., 2010; Saeki et al., 1979) and widely reported in various regions/transient structures in the near-Earth space including the plasma sheet boundary layer (Matsumoto et al., 1994; Norgren et al., 2015), auroral region (Ergun et al., 1998; Franz et al., 2005; Mozer et al., 1997), inner magnetosphere (Malaspina et al., 2014, 2018; Mozer et al., 2015; Vasko et al., 2015; Vasko, Agapitov, Mozer, Artemyev, Drake, et al., 2017), reconnection current sheets (Cattell et al., 2002, 2005; Graham et al., 2016), fast plasma flows (Deng et al., 2010; Ergun et al., 2015; Viberg et al., 2013), magnetic flux ropes (Khotyaintsev et al., 2010; Øieroset et al., 2014), and other regions of the near-Earth space (e.g., Cattell et al., 2003; Malaspina & Hutchinson, 2019; Mangeney et al., 1999; Pickett et al., 2008). In all these regions

electron phase space holes substantially contribute to the power spectral density of broadband electrostatic fluctuations reported already aboard early spacecraft missions (Gurnett et al., 1976; Lakhina et al., 2000; Scarf et al., 1974). Numerical simulations and theoretical analysis demonstrated that electron phase space holes can provide anomalous resistivity (Büchner & Elkina, 2006; Drake et al., 2003; Goldman et al., 2008), electron heating (Che et al., 2009, 2010, 2013; Drake et al., 2003), resonant acceleration (Artemyev et al., 2017; Kuzichev et al., 2017; Vasko, Kuzichev, et al., 2017), and pitch angle scattering (Vasko, Agapitov, Mozer, Artemyev, Krasnoselskikh, et al., 2017; Vasko, Krasnoselskikh, et al., 2018); produce Cherenkov emission of whistler waves (Goldman et al., 2014); and might be involved into electron surfing acceleration in collisionless shocks (Hoshino & Shimada, 2002; Schmitz et al., 2002). The experimental studies of electron phase space holes are also stimulated by a perspective of using these solitary waves as tracers of the reconnection process and plasma instabilities operating on time scales not resolved by plasma instruments (Khotyaintsev et al., 2010; Lapenta et al., 2011; Norgren et al., 2015).

Although single-spacecraft measurements supplied valuable information on properties of electron phase space holes (e.g., reviews by Franz et al., 2005; Hutchinson, 2017; Mozer et al., 2015; Pickett et al., 2004), the Magnetospheric Multiscale (MMS) mission has recently provided an opportunity for the most detailed analysis of electron phase space holes using multispacecraft observations with truly 3-D electric field measurements and record temporal resolution of the plasma measurements (Burch et al., 2016). In particular, the MMS measurements have already allowed resolving the three-dimensional structure of electron phase space holes (Holmes et al., 2018; Steinvall, Khotyaintsev, Graham, Vaivads, Lindqvist, et al., 2019; Tong et al., 2018), measuring the dearth of the phase space density of trapped electrons (Mozer et al., 2018), and resolving electromagnetic structure of subrelativistic electron phase space holes (Le Contel et al., 2017). In addition, the measurements of the MMS spacecraft allowed detecting whistler waves emitted by electron phase space holes via the Cherenkov resonance (Steinvall, Khotyaintsev, Graham, Vaivads, Le Contel, et al., 2019) and identifying electron acceleration and thermalization associated with electron phase space holes (Khotyaintsev et al., 2020; Mozer, Agapitov, Artemyev, et al., 2016; Mozer, Artemyev, Agapitov, et al., 2016; Norgren et al., 2020).

The critical issue that is not entirely resolved in the physics of electron phase space holes concerns the factors restricting or controlling velocity, amplitude and spatial scales of electron holes. In particular, Pickett et al. (2004) presented analysis of electrostatic solitary waves measured in various regions of the near-Earth space and demonstrated that the solitary waves tend to have larger amplitudes in regions with larger background magnetic fields. The physics behind that tendency was not properly considered though. Several case studies demonstrated that electron phase space holes in the Earth's magnetotail can have velocities comparable to a local ion thermal velocity (e.g., Cattell et al., 2003; Norgren, André, Vaivads, & Khotyaintsev, 2015) or electron thermal velocity (e.g., Cattell et al., 2005; Holmes et al., 2018; Tong et al., 2018). However, there is currently absent understanding of factors controlling separation between fast and slow electron phase space holes as well as of the relation between electron phase space holes of the different types. The understanding of the properties of electron holes and factors controlling the properties of electron holes would be valuable for predicting electron phase space hole parameters in space plasma environments, where in situ measurements are limited or not available, and using these solitary waves as tracers of instabilities not resolved by plasma instruments. The MMS measurements allow a thorough statistical analysis of electron phase space holes in a wide range of velocities, because the multispacecraft interferometry can be used to accurately estimate velocity and other parameters of electron phase space holes (see case studies presented by Holmes et al., 2018; Norgren, André, Vaivads, & Khotyaintsev, 2015; Steinvall, Khotyaintsev, Graham, Vaivads, Lindqvist, et al., 2019; Tong et al., 2018), which would not be feasible with single-spacecraft measurements.

In this paper we present a statistical analysis of more than 8,300 electrostatic solitary waves measured aboard MMS1 in the Earth's magnetotail with the major focus on analysis of more than 2,400 of these solitary waves measured aboard several (at least three) MMS spacecraft and interpreted in terms of electron phase space holes. In section 2 we describe the data, methodology and collected data set. In sections 3 and 4 we present case studies and results of the statistical analysis. In section 5 we provide theoretical estimates, interpretation and several implications of the presented results. We conclude with a summary of the presented results.

## 2. Data Set and Methodology

We use measurements in the burst mode of the following instruments aboard the MMS spacecraft: DC-coupled magnetic field at 128 S/s (samples per second) resolution provided by the Digital and Analogue Flux Gate Magnetometer (Russell et al., 2016), electric field at 8,192 S/s resolution provided by Axial Double Probe (Ergun et al., 2016) and Spin-Plane Double Probe (Lindqvist et al., 2016), electron and ion moments at 30 and 150 ms cadence provided by the Fast Plasma Instrument (Pollock et al., 2016). To collect a statistically representative data set of electron phase space holes, we considered several burst mode intervals around fast plasma flows in the Earth's magnetotail, where a copious amount of electron phase space holes is expected according to previous single-spacecraft measurements (Cattell et al., 2005; Deng et al., 2010; Ergun et al., 2015; Viberg et al., 2013). The selected intervals are listed in Table 1, while detailed overviews of these intervals can be found in the supporting information.

We select bipolar electrostatic solitary waves using an automatic algorithm that is accompanied by a visual test of the selected solitary waves. First, the automatic algorithm scans the parallel electric field  $E_{\parallel}$  measured by MMS1 and selects only spikes with amplitudes larger than 2 mV/m to exclude electric field fluctuations, which amplitudes are smaller than typical accuracy ( $\sim 1$  mV/m) of parallel electric field measurements. The electric field spikes, whose parallel electric field is well correlated with a model bipolar profile, are classified as bipolar electrostatic solitary waves and selected for further analysis. More specifically, the electric field of a spike is considered over the time interval of  $5\tau_{pp}$ , where  $\tau_{pp}$  is a peak-to-peak width of the spike (time delay between positive and negative peaks of  $E_{\parallel}$ ), and correlated with a model bipolar profile  $(t - t_0) \cdot \exp(-2(t - t_0)^2 / \tau_{pp}^2)$ , where  $t_0$  corresponds to  $E_{\parallel} = 0$ . The spike is classified as bipolar provided the correlation coefficient is larger than 0.6, and the results of the correlation analysis are tested visually to exclude inappropriate events. Second, for a solitary wave measured by MMS1 at some moment, the automatic algorithm selects parallel electric fields measured by MMS1–MMS4 over up to 100 ms around that moment and performs cross correlation between the  $E_{\parallel}$  signal measured by MMS1 and the  $E_{\parallel}$  signals measured by MMS2–MMS4. Because typical magnetic field-aligned spatial separations between MMS spacecraft is from a few kilometers to about 10 km, the minimum resolved velocity in the spacecraft frame is as low as about 100 km/s. The  $E_{\parallel}$  signals measured by MMS2–MMS4, which provide larger than 0.9 correlation coefficient with the  $E_{\parallel}$  signal measured by MMS1, are used to select bipolar  $E_{\parallel}$  signals potentially corresponding to the solitary wave measured aboard MMS1. For further analysis we considered only cases with the  $E_{\parallel}$  signals measured by at least two of MMS2–MMS4 being well correlated with the  $E_{\parallel}$  signal measured by MMS1. Third, to prove that the selected bipolar signals measured by different MMS spacecraft indeed correspond to the solitary wave propagated from one spacecraft to another, we use the two-spacecraft interferometry with MMS1 being a reference spacecraft. Under the assumption of magnetic field-aligned propagation of the solitary wave, we obtain velocity estimates  $V_{1i}$  using pairs of spacecraft (MMS1, MMS*i*) with well correlated  $E_{\parallel}$  signals:  $V_{1i} = \Delta z_{1i} / \Delta t_{1i}$ , where  $\Delta t_{1i}$  is the time delay between the  $E_{\parallel}$  signals measured by MMS1 and MMS*i*, while  $\Delta z_{1i}$  is the spatial separation between MMS1 and MMS*i* in the direction parallel to a local magnetic field. We note that before performing the cross correlation of  $E_{\parallel}$  signals measured aboard MMS1 and MMS*i* the  $E_{\parallel}$  signals are up sampled by a factor of 100 to increase the accuracy of estimates of time delays  $\Delta t_{1i}$ . We accept that the bipolar  $E_{\parallel}$  signals measured by different MMS spacecraft correspond to the solitary wave propagated from one spacecraft to another if the velocity estimates based on different pairs of MMS spacecraft are consistent with each other within 30%. The averaged value  $V_{ESW}$  of the velocity estimates  $V_{1i}$  is assumed to be the solitary wave velocity in the spacecraft frame.

We should comment on the assumption of magnetic field-aligned propagation of the solitary waves in the spacecraft frame. Numerous multidimensional simulations of electron streaming instabilities demonstrated that electron phase space holes seeded by these instabilities propagate parallel to the magnetic field in the plasma rest frame (Goldman et al., 1999; Huang et al., 2014; Miyake et al., 1998; Umeda et al., 2006; Wu et al., 2010). We selected solitary waves around fast plasma flows, where the perpendicular component of the plasma flow velocity can be a few hundred km/s (supporting information). Therefore, the solitary waves could be expected to propagate generally oblique to the magnetic field in the spacecraft frame. Clearly, for strictly one-dimensional solitary waves the only velocity component measurable by the interferometry is the component along the wave vector that is, in turn, parallel to the magnetic field, but in reality solitary

**Table 1**  
*List of the Fast Flow Event Considered in the Statistical Analysis*

No.	Date	Time	ESW observed on		
			One spacecraft	Three spacecraft	Four spacecraft
1	2017-07-29	15:45–16:10	905	538	232
2	2017-08-04	16:15–17:10	895	280	216
		19:10–19:25	641	234	68
		09:00–09:10	3,339	162	119
3	2017-08-06	05:09–05:16	265	30	21
		09:21–09:33	576	141	88
4	2017-08-07	16:00–17:00	1,776	1,041	638
		Total	8,388	2,426	1,382

*Note.* Dates are formatted as yyyy-mm-dd.

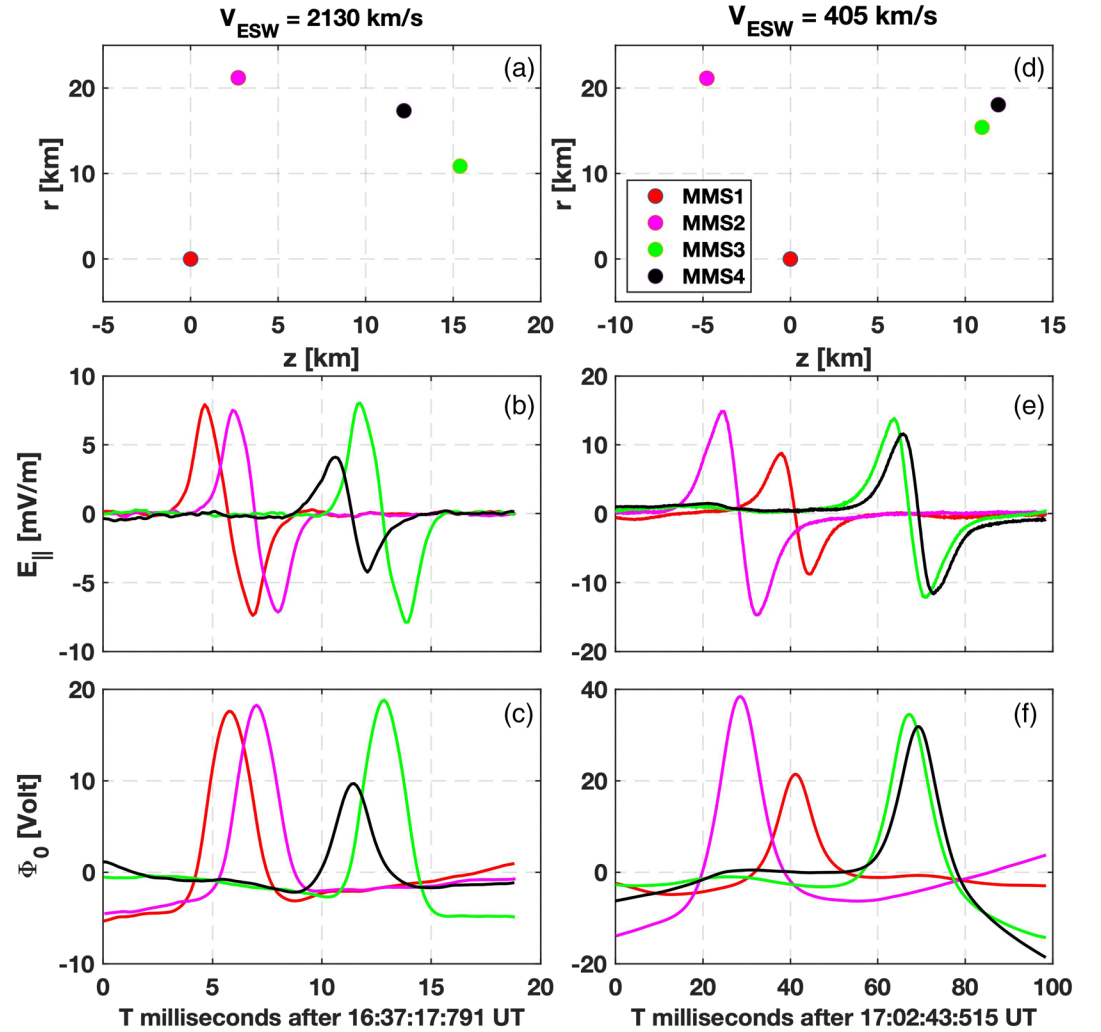
waves are three-dimensional structures with some perpendicular spatial scale (Ergun et al., 1999; Franz et al., 2000; Holmes et al., 2018; Steinvall, Khotyaintsev, Graham, Vaivads, Lindqvist, et al., 2019; Tong et al., 2018). The assumption of magnetic field-aligned propagation in the spacecraft frame excludes from consideration solitary waves, which are swept by the perpendicular plasma flow by more than typical perpendicular spatial scale during the solitary wave propagation from one spacecraft to another. In other words, that assumption restricts the analysis to solitary waves, which appear as approximately one-dimensional, though they are certainly three-dimensional structures. In this study we do not consider the three-dimensional structure of electrostatic solitary waves but concentrate on analysis of  $E_{\parallel}$  of the solitary waves measured aboard several MMS spacecraft. The statistical analysis of the three-dimensional structure of the solitary waves is left for future studies.

Table 1 shows that in the selected burst mode intervals we have identified 8,388 bipolar electrostatic solitary waves measured aboard MMS1. We have identified 2,426 solitary waves measured aboard several (at least three) MMS spacecraft and found that 1,382 of these solitary waves were actually measured aboard four MMS spacecraft. We note that the data set of solitary waves measured aboard several MMS spacecraft includes only solitary waves with positive electrostatic potentials, which will be referred by electron phase space holes or electrons holes in what follows. About 20 solitary waves were excluded from the original data set of solitary waves measured aboard several MMS spacecraft, because they had negative electrostatic potentials and were most likely ion phase space holes (see Børve et al., 2001; Bounds et al., 1999; McFadden et al., 2003; Schamel, 1986; Wang et al., 2020, for measurements and simulations of ion holes).

In the next section we present case studies and results of the statistical analysis of the electron holes measured aboard several MMS spacecraft. The electron hole amplitudes are compared to ion and electron parallel temperatures  $T_i$  and  $T_e$ , while the parallel scales are compared to a local Debye length  $\lambda_D = (T_e/4\pi n_e e^2)^{1/2}$ , where  $n_e$  is the electron density,  $e$  is the electron charge. The electron hole velocities in the plasma rest frame are computed as  $V_{ESW} - V_{\parallel i}$ , where  $V_{\parallel i}$  is the ion bulk velocity parallel to a local magnetic field. The ion bulk velocity  $V_{\parallel i}$  can be comparable to  $V_{ESW}$  (supporting information) and, hence, need to be taken into account to accurately determine electron hole velocities in the plasma rest frame. Because the electron holes have typical duration of the order of a few milliseconds, while electron and ion moments are available at 30 and 150 ms cadence, we use electron and ion moments measured by MMS1 at the time instant closest to the electron hole occurrence aboard MMS1.

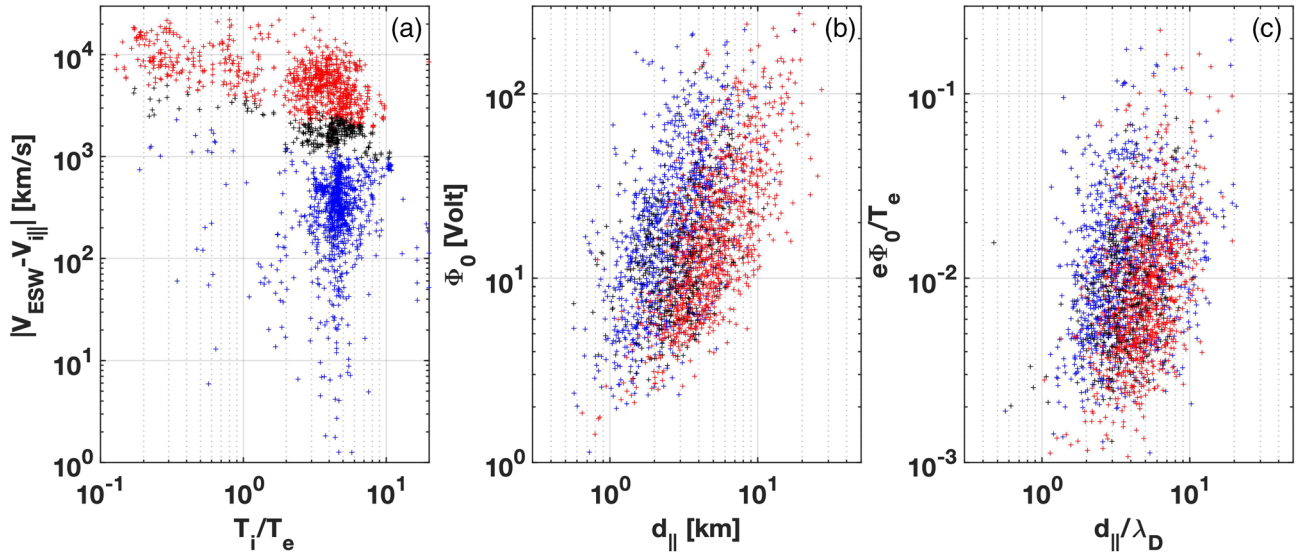
### 3. Statistical Analysis of Electron Hole Velocities, Spatial Scales, and Amplitudes

Figure 1 presents the analysis of a couple of bipolar electrostatic solitary waves measured aboard four MMS spacecraft around 16:37 and 17:02 UT on 7 August 2017. Panels (a) and (d) demonstrate the position of the MMS spacecraft with respect to MMS1 and show that the spatial separations between the MMS spacecraft in the directions parallel and perpendicular to a local magnetic field were within 20 km. Panels (b) and (e) present the parallel electric fields  $E_{\parallel}$  measured by MMS1–MMS4. The occurrence of the bipolar  $E_{\parallel}$  signals aboard the MMS spacecraft is consistent with the spacecraft positions provided that the solitary wave propagates parallel to the local magnetic field direction. Three velocity estimates obtained by the two-spacecraft



**Figure 1.** The analysis of a couple of electron holes measured aboard four MMS spacecraft on 7 August 2017. The upper panels (a, d) present the spacecraft position with respect to MMS1 and demonstrate the spatial separations between the MMS spacecraft in the direction parallel to a local magnetic field (along the  $z$  axis) and in the plane perpendicular to the magnetic field ( $r$  is the distance in that plane). The middle panels (b, e) present the electric fields measured aboard the MMS spacecraft. The analysis of time delays  $\Delta t_{1i}$  between bipolar  $E_{||}$  signals measured aboard MMS1 and MMS $i$  allows us to obtain three estimates of the electron hole velocity  $V_{1i} = \Delta z_{1i} / \Delta t_{1i}$ , where  $\Delta z_{1i}$  is the separation between MMS1 and MMS $i$  along the magnetic field. For electron hole in Panel (b) we have  $(V_{12}, V_{13}, V_{14}) = (385, 415, 413)$  km/s, while for electron hole in Panel (e) we have  $(V_{12}, V_{13}, V_{14}) = (2,066, 2,161, 2,162)$  km/s, so that three velocity estimates are consistent with each other. The averaged value of  $V_{12}$ ,  $V_{13}$  and  $V_{14}$  is assumed to be electron hole velocity  $V_{ESW}$  that is shown above the upper panels. The estimated velocity allows estimating the parallel spatial scales of the electron holes (section 3 for details). The bottom panels (c, f) present the electrostatic potentials observed aboard each MMS spacecraft that was computed as  $\Phi^{(i)} = \int E_{||} V_{ESW} dt$ , where index  $i$  corresponds to MMS $i$ .

interferometry are provided in the caption to Figure 1. The smallest and the largest of the velocity estimates indicate the accuracy of the averaged solitary wave velocity. The velocity of the solitary wave in Panel (b) is in the range from 2,060 to 2,160 km/s, while the averaged velocity is  $V_{ESW} \approx 2,130$  km/s. The velocity of the solitary wave in Panel (e) is in the range from 385 to 415 km/s, while the averaged velocity is  $V_{ESW} \approx 405$  km/s. The parallel spatial scales observed aboard individual MMS spacecraft are computed as  $d_{||}^{(i)} = 0.5 V_{ESW} \cdot \tau_{pp}^{(i)}$ , where  $\tau_{pp}^{(i)}$  is the time delay between minimum and maximum values of the bipolar  $E_{||}$  signal measured aboard MMS $i$  (peak-to-peak temporal width). The typical parallel spatial scale  $d_{||}$  is computed by averaging spatial scales  $d_{||}^{(i)}$  observed aboard individual MMS spacecraft. We have found  $d_{||} \approx 2$  km for the solitary wave



**Figure 2.** The parameters of 2,426 electron holes measured aboard at least three MMS spacecraft in the burst mode intervals indicated in Table 1: (a) electron hole velocities in the plasma rest frame versus ion to electron temperature ratio  $T_i/T_e$ , where  $T_i$  and  $T_e$  are local ion and electron parallel temperatures measured aboard MMS1 at the time instant closest to electron hole occurrence aboard MMS1; (b) electrostatic potential amplitudes  $\Phi_0$  of the electron holes versus parallel spatial scales  $d_{||}$  (amplitude and spatial scale are computed as averaged values of corresponding quantities observed aboard three or four MMS spacecraft); (c)  $e\Phi_0/T_e$  versus  $d_{||}/\lambda_D$ , where  $\lambda_D$  is a local Debye length. In all panels red dots correspond to fast electron holes,  $|V_{ESW} - V_{||}| > 0.1 V_{Te}$ , blue dots correspond to slow electron holes,  $|V_{ESW} - V_{||}| < 0.05 V_{Te}$ , and black dots correspond to medium electron holes with velocities between 0.05 and 0.1  $V_{Te}$ , where  $V_{Te} = (2T_e/m_e)^{1/2}$  is electron thermal velocity.

in Panel (b) and  $d_{||} \approx 1.4$  km for the solitary wave in Panel (e), while in units of local Debye lengths  $d_{||} \approx 2\lambda_D$  and  $3\lambda_D$ , respectively. We use the averaged velocities to compute electrostatic potentials observed aboard individual MMS spacecraft as  $\Phi^{(i)} = \int E_{||} V_{ESW} dt$ , where superscript  $i$  corresponds to MMS $i$ . Panels (c) and (f) demonstrate that the solitary waves can be referred by electron holes, because of positive electrostatic potentials. The amplitudes of electrostatic potentials are of a few tens of volts that is much smaller than a local electron temperature of 1 keV and a local ion temperature of 5 keV. We characterize electron holes by typical amplitude  $\Phi_0$  computed by averaging maximum values  $\Phi_0^{(i)}$  of electrostatic potentials observed aboard individual MMS spacecraft. We recall that the two-spacecraft interferometry provides estimates of the solitary wave velocity in the spacecraft rest frame. During observations of electron holes shown in Panels (b) and (e) the plasma flow velocity parallel to a local magnetic field  $V_{||}$  was about 650 and 340 km/s, that is why the electron hole velocities in the plasma rest frame  $V_{ESW} - V_{||}$  were about 1,500 and 65 km/s, respectively. In this section we present results of the statistical analysis of 2,426 electron holes observed aboard at least three MMS spacecraft.

Figure 2 presents velocities, parallel spatial scales and amplitudes of the electron holes. Panel (a) shows ion to electron temperature ratio  $T_i/T_e$  corresponding to each of the electron holes and velocities  $|V_{ESW} - V_{||}|$  in the plasma rest frame. The majority of the electron holes were measured at  $T_i/T_e \approx 3-10$ , which is typical of the Earth's magnetotail plasma sheet (e.g., Artemyev et al., 2011), while about 10% of the electron holes were measured at  $T_i/T_e \lesssim 1$ , which most likely corresponds to MMS measurements in the magnetotail lobes, because smaller values of  $T_i/T_e$  tend to be at smaller electron densities and ion temperatures (supporting information). The electron hole velocities in the plasma rest frame are in the range from just a few km/s up to 20,000 km/s. We classified the electron holes into slow electron holes with  $|V_{ESW} - V_{||}| < 0.05 V_{Te}$ , fast electron holes with  $|V_{ESW} - V_{||}| > 0.1 V_{Te}$ , and medium electron holes with  $0.05 V_{Te} < |V_{ESW} - V_{||}| < 0.1 V_{Te}$ , where  $V_{Te} = (2T_e/m_e)^{1/2}$  is the electron thermal velocity. Panel (a) shows that slow electron holes have velocities typically below 800 km/s, fast electron holes have velocities typically larger than 2,000 km/s, while medium electron holes have velocities clustered between slow and fast electron hole velocities. Panel (b) shows that the electron holes have amplitudes from a few volts up to a few hundred volts and parallel spatial scales from 0.5 to 30 km. Panel (c) shows that the parallel spatial scales  $d_{||}$  of the electron holes are

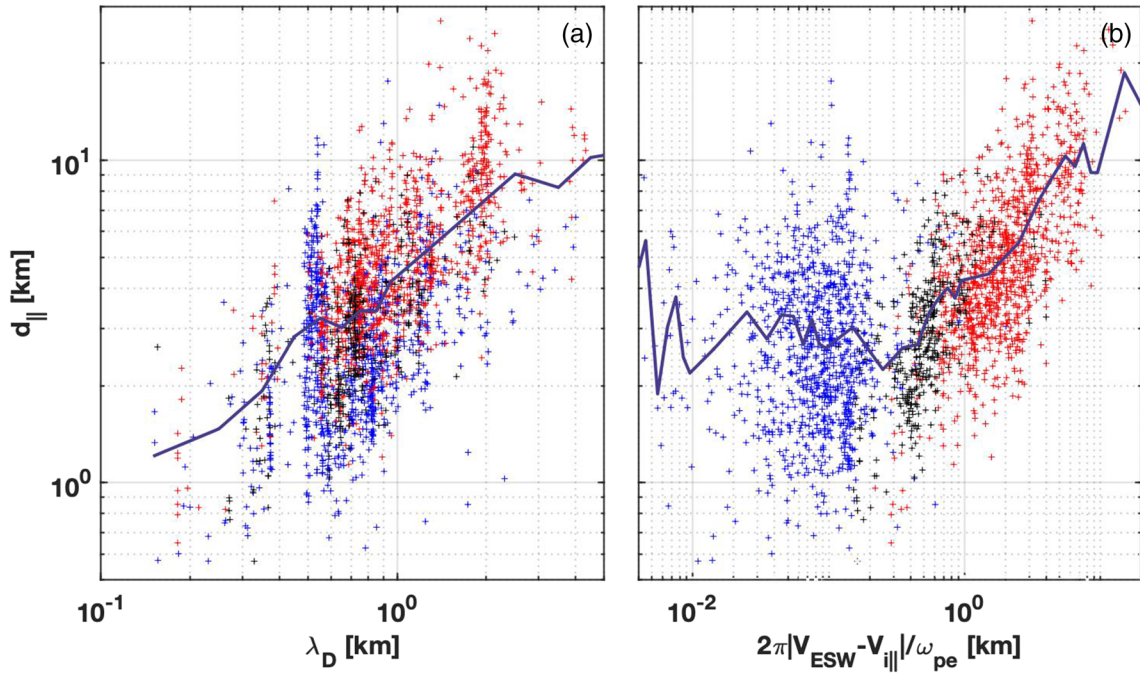


**Figure 3.** The analysis of factors controlling the parallel spatial scales of the electron holes: (a)  $d_{||}$  versus  $\lambda_D$  (local Debye length); (b)  $d_{||}$  versus  $2\pi|V_{ESW} - V_{||}|/\omega_{pe}$ , where  $\omega_{pe}$  is the electron plasma frequency (section 3 for details). In both panels blue, black, and red dots correspond to slow, medium, and fast electron holes. The solid curves in both panels are obtained by computing averaged values of  $d_{||}$  computed at various values of the parameters on the abscissa axes.

typically between  $\lambda_D$  and  $10\lambda_D$ , while the amplitudes  $e\Phi_0$  are typically between  $10^{-3} T_e$  and  $0.1 T_e$ . One can see in Panel (b) that the electron holes with larger parallel spatial scales tend to have larger amplitudes, while no similar trend is observed between normalized amplitudes and spatial scales in Panel (c). Panels (b) and (c) show that slow and fast electron holes are not different in terms of amplitudes and parallel spatial scales, though statistically fast electron holes have a few times larger parallel spatial scales than slow electron holes. The larger parallel spatial scales of fast electron holes cannot be an artifact of the selection procedure (see discussion below).

Figure 3 addresses the parallel spatial scales of the electron holes. Panel (a) demonstrates that the parallel spatial scale  $d_{||}$  tend to be larger for larger local Debye length  $\lambda_D$ , indicating thereby that the local Debye length determines the parallel spatial scale of the electron holes. We should note that a positive correlation between  $d_{||}$  and  $\lambda_D$  is not well noticeable for slow electron holes, because for these electron holes  $\lambda_D$  is in a rather narrow range from 0.5 to 0.9 km. Panel (b) compares the parallel spatial scale  $d_{||}$  to  $2\pi|V_{ESW} - V_{||}|/\omega_{pe}$ , where  $\omega_{pe} = (4\pi n_e e^2/m_e)^{1/2}$  is the electron plasma frequency. There is a distinct positive correlation between  $d_{||}$  and  $2\pi|V_{ESW} - V_{||}|/\omega_{pe}$  for fast electron holes, whereas no correlation between these quantities is observed for slow electron holes. The increase of  $d_{||}$  with increasing  $2\pi|V_{ESW} - V_{||}|/\omega_{pe}$  for fast electron holes and absence of similar trend for slow electron holes cannot be an artifact of the solitary wave selection procedure. The analysis in section 4 shows that bipolar  $E_{||}$  profiles of fast and slow electron holes are well resolved by MMS measurements (8,192 S/s corresponds to 0.12 ms cadence), because peak-to-peak widths  $\tau_{pp}$  of slow electron holes are typically (>95% of cases) larger than 3 ms, while temporal widths of fast electron holes are typically larger than 0.7 ms (Figure 6). We may certainly miss too fast electron holes with temporal widths  $\tau_{pp}$  less than a few of 0.12 ms, but fast electron holes, which are well resolved by MMS, clearly show the positive correlation between  $d_{||}$  and  $2\pi|V_{ESW} - V_{||}|/\omega_{pe}$ .

Figure 4 addresses the factors controlling the electron hole velocities. Panel (a) presents the distribution of electron holes in the parameter plane of  $|V_{ESW} - V_{||}|$  and  $\Phi_0$  and demonstrates the absence of any dependence between the electron hole velocity and amplitude. In physical units the electron hole velocities more or less continuously cover the range from a few km/s up to 20,000 km/s. Panel (b) shows the distribution of electron holes in similar parameter plane, but with electron hole velocities normalized to a local ion thermal

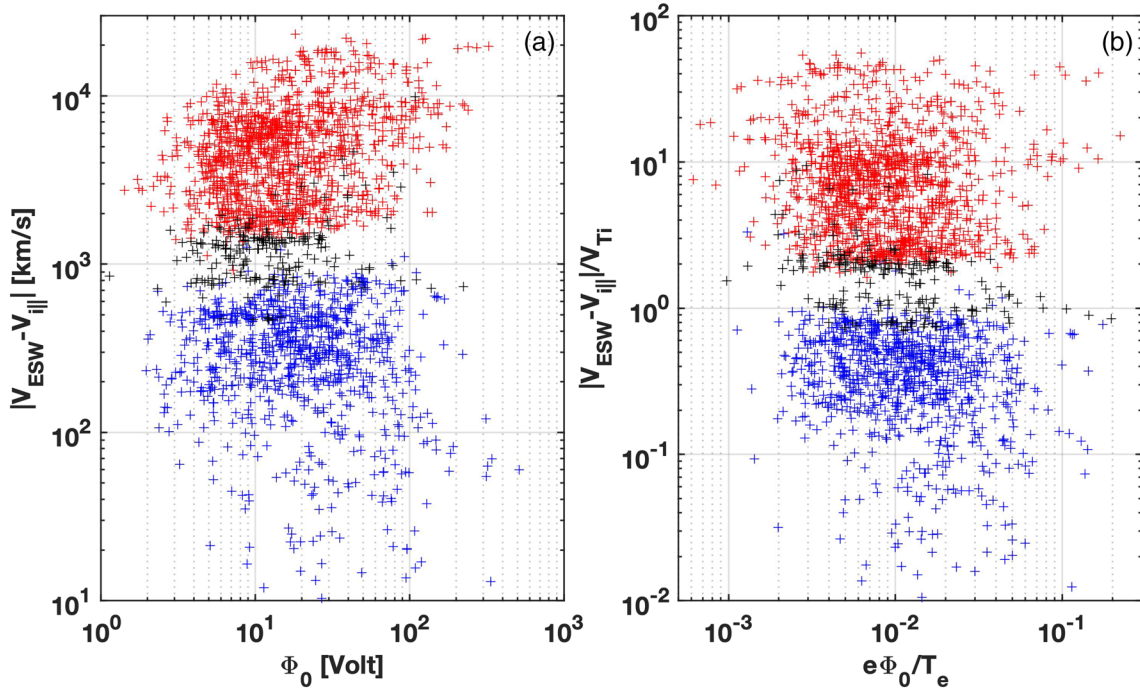


**Figure 4.** The analysis of factors controlling velocities of the electron holes: (a) electron hole velocity in the plasma rest frame  $|V_{ESW} - V_{||}|$  versus amplitude  $\Phi_0$ ; (b)  $|V_{ESW} - V_{||}|/V_{Ti}$  versus  $e\Phi_0/T_e$ , where  $V_{Ti}$  is local ion thermal velocity. In both panels blue, black, and red dots correspond to slow, medium, and fast electron holes, respectively.

velocity  $V_{Ti} = (2T_i/m_i)^{1/2}$  and electron hole amplitudes normalized to a local electron temperature  $T_e$ . An interesting feature in Panel (b) is a gap in the distribution of electron hole velocities at  $V_{Ti} \lesssim |V_{ESW} - V_{||}| \lesssim 2V_{Ti}$ . That gap was hardly visible in the distribution of electron hole velocities in physical units in Panel (a). Almost all slow electron holes have velocities below a local ion thermal velocity,  $|V_{ESW} - V_{||}| \lesssim V_{Ti}$ , while almost all fast electron holes have velocities 2 times larger than the ion thermal velocity,  $|V_{ESW} - V_{||}| \gtrsim 2V_{Ti}$ . Noteworthy that the normalization of  $|V_{ESW} - V_{||}|$  to  $V_{Ti}$  split the class of medium electron holes in those with  $|V_{ESW} - V_{||}| \gtrsim 2V_{Ti}$  and  $|V_{ESW} - V_{||}| \lesssim V_{Ti}$ . The physics behind the observed influence of the ion thermal motion on the electron hole velocities is clarified in section 5.

The collected data set can be used to address the role of the transverse electron hole instability in restricting electron hole amplitudes. The theoretical studies and numerical simulations demonstrated that one-dimensional electron holes are unstable to the transverse instability provided that the bounce frequency of electrons trapped within the bipolar parallel electric field,  $\omega_{be} = d_{||}^{-1} (e\Phi_0/m_e)^{1/2}$ , substantially exceeds a local electron cyclotron frequency  $\omega_{ce} = eB_0/m_e c$  (Hutchinson, 2018, 2019; Muschietti et al., 2000; Umeda et al., 2006; Wu et al., 2010). Therefore, the bounce frequency of electrons trapped in the observed electron holes is expected to be below the transverse instability threshold,  $\omega_{be} \lesssim \gamma \omega_{ce}$ , where  $\gamma$  is the parameter of the order of 1 dependent on a specific model electric field profile adopted in the transverse instability analysis (Hutchinson, 2019). The stability criterion  $\omega_{be} \lesssim \gamma \omega_{ce}$  can be written in the form of an upper threshold on the electron hole amplitude

$$e\Phi_0 \lesssim \gamma^2 m_e \omega_{ce}^2 d_{||}^2 \quad (1)$$

We will test the collected electron holes against that stability criterion with  $\gamma = 1$  and 1.5, which were reported in the numerical simulations (Hutchinson, 2019; Muschietti et al., 2000).

Figure 5 demonstrates the analysis of the transverse instability criterion of the electron holes. Panel (a) presents the comparison between  $e\Phi_0$  and  $m_e \omega_{ce}^2 d_{||}^2$  and shows that slow, medium and fast electron holes indeed satisfy the stability criterion given by Equation 1. Moreover, the electron holes with  $m_e \omega_{ce}^2 d_{||}^2 \lesssim 100$  eV



demonstrate that the upper threshold on the electron hole amplitude is better described by Equation 1 with  $r = 1.5$ . Panel (b) presents the test of the stability criterion given by Equation 1 with parameters  $\Phi_0^{(i)}$  and  $d_{\parallel}^{(i)}$  and shows that the electron hole parameters measured aboard individual MMS spacecraft also satisfy the stability criterion. Noteworthy that a substantial fraction of the electron holes is well below the transverse instability threshold, which implies that this instability is not involved into restricting the amplitude of these electron holes. We have noticed that  $\omega_{pe}/\omega_{ce}$  is a critical parameter, which determines whether or not the transverse instability is involved into restricting electron hole amplitudes. Panel (c) presents the test of the stability criterion given by Equation 1, where electron holes were split into those observed at  $\omega_{pe}/\omega_{ce} > 10$  and  $\omega_{pe}/\omega_{ce} < 10$ . Panel (c) shows that the electron holes observed at  $\omega_{pe}/\omega_{ce} < 10$  are well below the transverse instability threshold. In contrast, some of the electron holes observed at  $\omega_{pe}/\omega_{ce} > 10$  are around the transverse instability threshold and, hence, amplitudes of these electron holes can be controlled by the transverse instability. The physics behind that critical role of parameter  $\omega_{pe}/\omega_{ce}$  is clarified in section 5.

#### 4. Statistical Analysis of Temporal Characteristics of Electron Holes

In this section we present analysis of temporal characteristics of 8,388 electrostatic solitary waves collected using  $E_{\parallel}$  measurements aboard MMS1 and 2,426 of these solitary waves measured aboard several MMS spacecraft and interpreted in terms of electron phase space holes (Table 1). We consider peak-to-peak temporal widths  $\tau_{pp}$  of the electron holes defined as the time delay between minimum and maximum values of  $E_{\parallel}$  measured aboard MMS1. We determine statistical distributions of time intervals  $\Delta t_{HH}$  between electron holes sequentially observed aboard MMS1. Finally, we provide lower bounds for electron hole lifetimes based on the maximum time delay  $\Delta t_{\max}$  between observations of the same electron hole aboard several MMS spacecraft and compare these lower bounds to typical plasma time scales such as  $\omega_{pe}^{-1}$  and  $\omega_{ce}^{-1}$ .

Figure 6 presents temporal characteristics of 2,426 electron holes measured aboard several MMS spacecraft. Panel (a) presents the cumulative distribution function (CDF) of peak-to-peak temporal widths  $\tau_{pp}$  of all 2,426 electron holes as well as analogous CDFs computed separately for fast and slow electron holes, which total numbers are 1,047 and 1,012, respectively. For more than 95% of all electron holes we have  $\tau_{pp} > 0.9$  ms, which demonstrates that electric field measurements at 8,192 S/s (cadence of 0.12 ms) well resolve electric field profiles of the most of the electron holes. The CDFs in Panel (a) clearly show that fast and slow electron holes have substantially different temporal widths, because  $\tau_{pp} < 3$  ms for about 95% of fast electron holes, while  $\tau_{pp} > 3$  ms for about 95% of slow electron holes. Panel (b) presents CDFs of time intervals  $\Delta t_{HH}$  between sequentially observed fast electron holes and sequentially observed slow electrons holes, while Panel (c) presents analogous CDF of time intervals between sequentially observed fast and slow electron holes. The CDF in Panel (c) shows that in 99% of cases the time interval between sequentially observed fast and slow electron holes is larger than 10 seconds. This strongly indicates that fast and slow electron holes are produced by instabilities, which are not statistically related with each other. The CDFs in Panel (b) show that  $\Delta t_{HH}$  is less than 100 ms (400 ms) for more than 60% (60%) of sequentially observed fast (slow) electron holes. Thus, fast (slow) electron holes are typically observed in groups, though some can be rather isolated, because  $\Delta t_{HH}$  is larger than a few seconds for about 10% of fast (slow) electron holes. These features of the temporal distribution of fast and slow electron holes are well noticeable by inspecting waveforms of  $E_{\parallel}$ .

The analysis presented in Figure 6 is restricted to electron holes measured aboard several MMS spacecraft. We performed similar analysis for 8,388 electrostatic solitary waves measured aboard MMS1 (Table 1). We recall that some fraction of 8,388 electrostatic solitary waves can have negative potentials and, hence, can be not electron holes. These solitary waves cannot be filtered out, because we computed the velocity only for solitary waves measured aboard several MMS spacecraft. The fraction of solitary waves with negative potentials is expected to be less than 1% though, because there were only about 20 solitary waves with negative potentials among more than 2,400 solitary waves measured aboard several MMS spacecraft (section 2).

Figure 7a presents the CDF of temporal widths of 8,386 solitary waves measured aboard MMS1 and indicates that  $\tau_{pp} < 3$  ms and  $\tau_{pp} > 3$  ms for 5562 (66.3%) and 2,826 (33.7%) solitary waves, respectively. The analysis in Figure 6 showed that more than 95% of the solitary waves with  $\tau_{pp} < 3$  ms should be fast electron holes and more than 95% of the solitary waves with  $\tau_{pp} > 3$  ms should be slow electron holes. Therefore, in what follows 5,562 solitary waves with  $\tau_{pp} < 3$  ms and 2,826 solitary waves with  $\tau_{pp} > 3$  ms are referred by “fast”

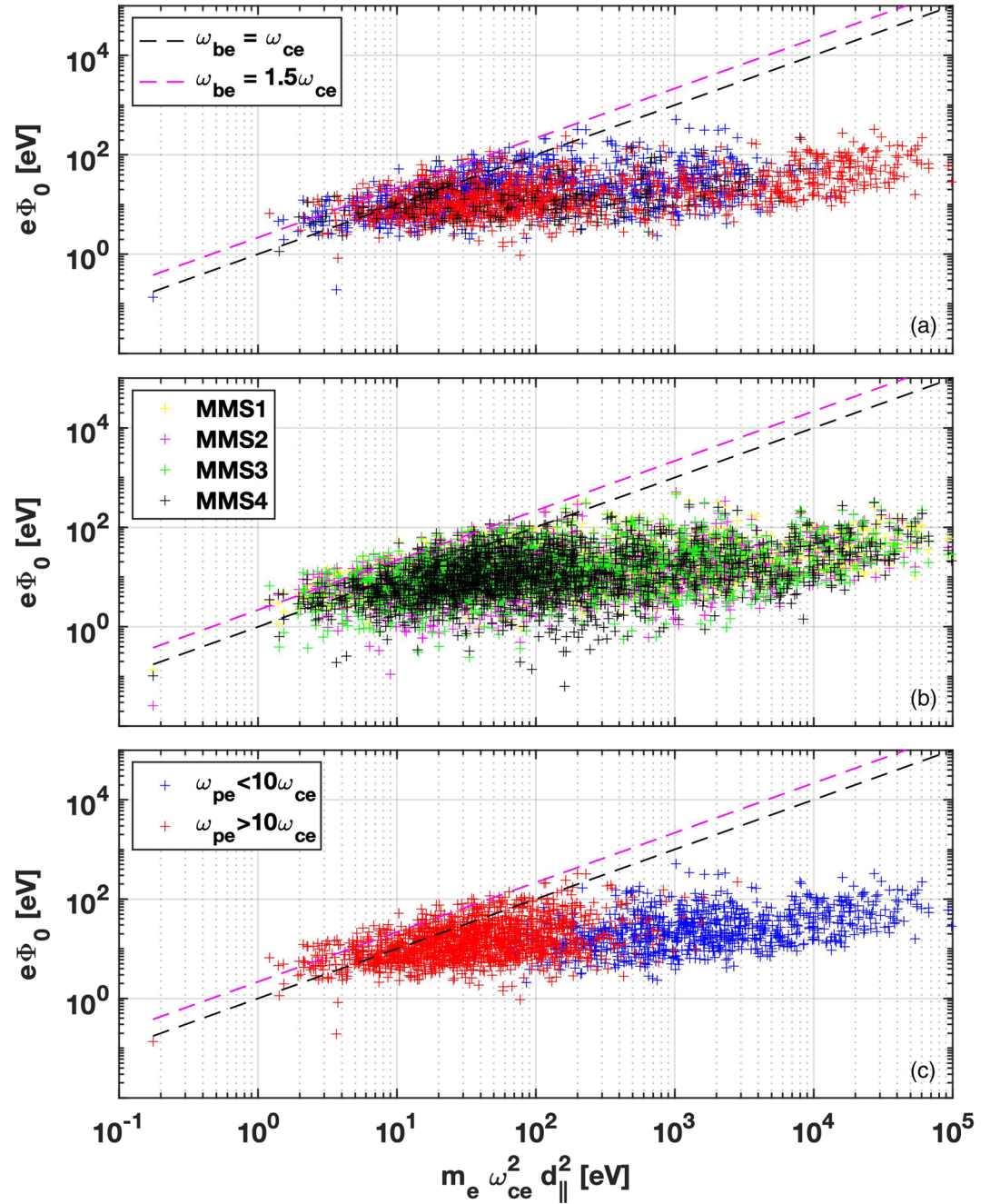


**Figure 5.** The analysis of the transverse instability criterion of the electron holes (see section 5 for details). To be stable with respect to the transverse instability the electron holes, in which lifetime is longer than about  $\omega_{ce}^{-1}$ , have to satisfy  $\omega_{be} \lesssim \gamma \omega_{ce}$  or, equivalently,  $e\Phi_0 \lesssim \gamma^2 m_e \omega_{ce}^2 d_{\parallel}^2$ , where  $\omega_{be} = d_{\parallel}^{-1} (e\Phi_0/m_e)^{1/2}$  is the bounce frequency of electrons trapped by electron hole, while  $\gamma$  should be of the order of 1 according to numerical simulations (Hutchinson, 2019; Muschietti et al., 2000). Panel (a) addresses the transverse instability using amplitude  $\Phi_0$  and parallel scale  $d_{\parallel}$ , which are averaged values of corresponding quantities observed aboard three or four MMS spacecraft. Panel (b) addresses the transverse instability using amplitudes  $\Phi_0^{(i)}$  and parallel spatial scales  $d_{\parallel}^{(i)}$  observed aboard individual MMS spacecraft ( $i = 1, 2, 3$  and  $4$ ). Panel (c) addresses the transverse instability using amplitude  $\Phi_0$  and parallel scale  $d_{\parallel}$ , but the electron holes were separated into those observed at  $\omega_{pe}/\omega_{ce} > 10$  and  $\omega_{pe}/\omega_{ce} < 10$ . The dashed lines in the panels represent transverse instability thresholds,  $\omega_{be} = \omega_{ce}$  and  $\omega_{be} = 1.5 \omega_{ce}$  (Hutchinson, 2019; Muschietti et al., 2000).

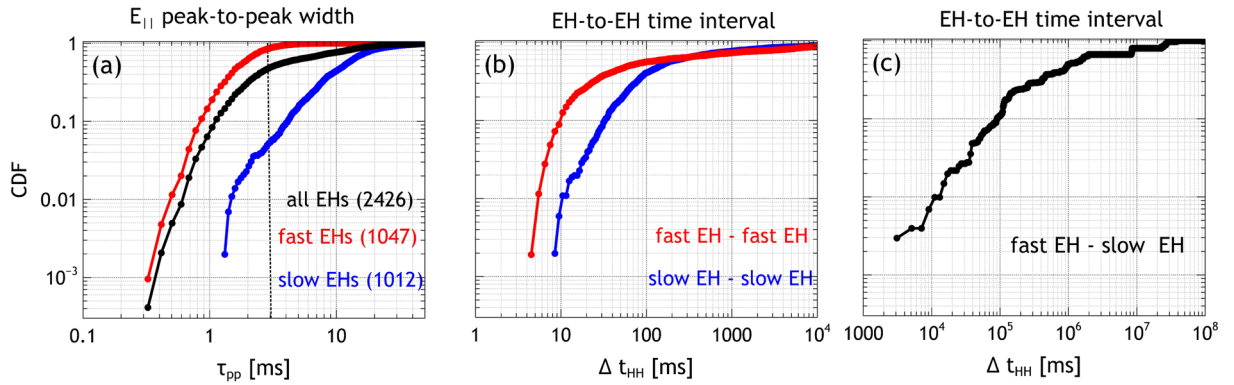


**Figure 6.** The analysis of temporal characteristics of 2,426 electron holes (EH) measured aboard at least three MMS spacecraft (Table 1). The panels present cumulative distribution functions (CDF) of (a) temporal peak-to-peak widths  $\tau_{pp}$  of bipolar  $E_{||}$  signals measured aboard MMS1 (peak-to-peak time delay); CDFs are presented separately for 1,047 fast electron holes ( $|V_{ESW} - V_{i||}| > 0.1V_{Te}$ ), 1,012 slow electron holes ( $|V_{ESW} - V_{i||}| < 0.05V_{Te}$ ), and all 2,426 electron holes; (b) time intervals  $\Delta t_{HH}$  between sequentially observed fast electron holes and sequentially observed slow electrons holes (EH-to-EH time delays); (c) time intervals  $\Delta t_{HH}$  between sequentially observed fast and slow electrons holes.

and “slow” electron holes, respectively. Figure 7b presents CDFs of time intervals between sequentially observed “fast” electron holes and sequentially observed “slow” electron holes. Interestingly, these CDFs are almost identical to CDFs of time intervals between fast electron holes and between slow electron holes shown in Figure 6b and duplicated in Figure 7b. First, this reinforces the point that  $\tau_{pp} = 3$  ms can be considered as a threshold value to distinguish between slow and fast electron holes in the Earth’s magnetotail. Second, this shows that CDFs presented in Figure 6b are not biased, in spite of the fact that these CDFs correspond to electron holes measured only aboard several MMS spacecraft. Panel (c) presents the CDF of time intervals between sequentially observed “fast” and “slow” electron holes and demonstrates that  $\Delta t_{HH}$  is larger than 10 s for more than 95% of cases. The comparison of that CDF to the CDF of time intervals between fast and slow electron holes, which is duplicated in Figure 7c, demonstrates that time intervals between fast and slow electron holes are statistically larger than between “fast” and “slow” electron holes. The difference between these CDFs is explained as follows. The threshold  $\tau_{pp} = 3$  ms does not ideally separates solitary waves into fast and slow electrons holes, because about 5% of “fast” electron holes can be actually slow and about 5% of “slow” electron holes can be actually fast (Figure 6). Therefore, some of sequentially observed “fast” and “slow” electron holes may be of the same type (fast or slow) resulting in statistically smaller time intervals between “fast” and “slow” electron holes than between fast and slow electron holes. In spite of the imperfect separation of fast and

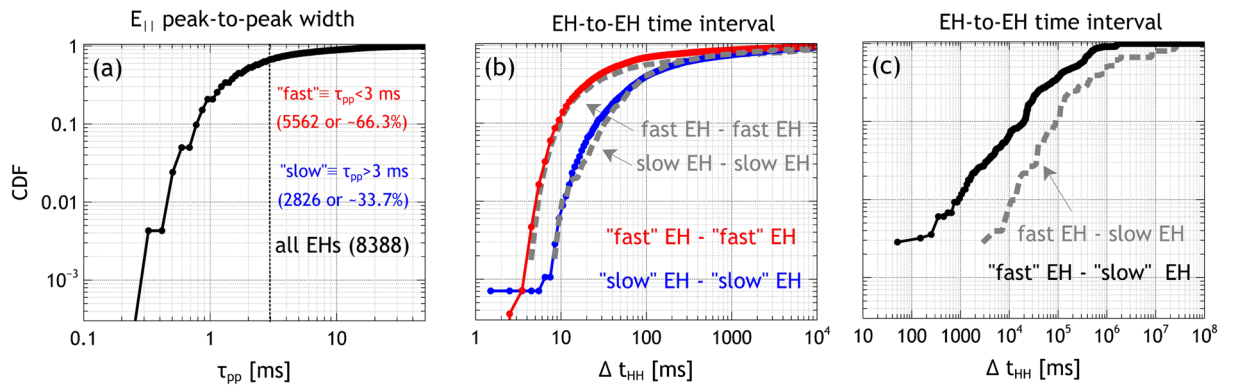


**Figure 7.** The analysis of temporal characteristics of 8,388 solitary waves measured aboard MMS1 (Table 1). The panels present cumulative distribution functions (CDF) of (a) peak-to-peak temporal widths  $\tau_{pp}$  of bipolar  $E_{||}$  signals measured aboard MMS1 for all 8,388 solitary waves; there are 5,562 solitary waves with  $\tau_{pp} < 3$  ms referred by “fast” electron holes and 2,826 solitary waves with  $\tau_{pp} > 3$  ms referred by “slow” electron holes; (b) time intervals  $\Delta t_{HH}$  between sequentially observed “fast” electron holes and sequentially observed “slow” electrons holes (EH-to-EH time delays); (c) time intervals  $\Delta t_{HH}$  between sequentially observed “fast” and “slow” electrons holes. In Panels (b) and (c) we duplicate CDFs for fast and slow electron holes presented in Figures 6b and 6c.

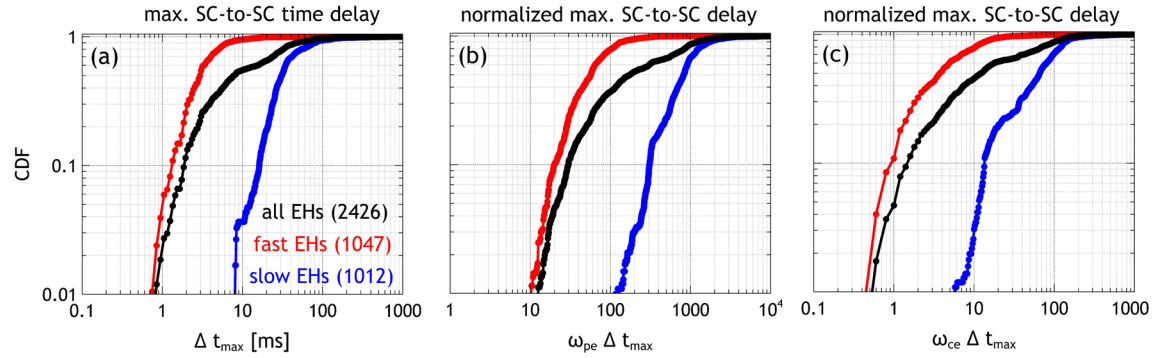


**Figure 8.** The analysis of lower bounds of electron hole lifetimes based on the data set of 2,426 electron holes measured aboard several MMS spacecraft (Table 1). The lowest estimate of the lifetime of an electron hole  $\Delta t_{\max}$  is determined as the maximum of the time delays  $\Delta t_{ij}$  between observations of the electron hole aboard different MMS spacecraft (MMS*i* and MMS*j*). Panel (a) presents CDFs of  $\Delta t_{\max}$  determined for fast, slow, and all 2,426 electron holes. Panels (b) and (c) present analogous CDFs for  $\omega_{pe}\Delta t_{\max}$  and  $\omega_{ce}\Delta t_{\max}$ , where  $\omega_{pe}$  and  $\omega_{ce}$  are local electron plasma and cyclotron frequencies.

slow electron holes using the temporal width, still Figure 7c confirms that fast and slow electron holes are not associated with each other and produced by instabilities not statistically related with each other.

Figure 8 presents the analysis of electron hole lifetimes using the data set of 2,426 electron holes measured aboard several MMS spacecraft. A lower bound for the lifetime of an electron hole is the time delay between observations of the electron hole aboard a pair of MMS spacecraft. For each of 2,426 electrons holes, we select the maximum time delay  $\Delta t_{\max}$  among time delays  $\Delta t_{ij}$  between observations of the same electron hole aboard MMS*i* and MMS*j*. Panels (a)–(c) present CDFs of  $\Delta t_{\max}$ ,  $\omega_{pe}\Delta t_{\max}$  and  $\omega_{ce}\Delta t_{\max}$  computed for fast, slow and all 2,426 electron holes. Panel (a) shows that  $\Delta t_{\max}$  is typically between 1 and 10 ms for fast electron holes and between 10 and 100 ms for slow electrons holes. Panel (b) demonstrates that typically ( $5\% \lesssim \text{CDF} \lesssim 95\%$ ) we have  $20 \omega_{pe}^{-1} \lesssim \Delta t_{\max} \lesssim 100 \omega_{pe}^{-1}$  for fast electron holes and  $300 \omega_{pe}^{-1} \lesssim \Delta t_{\max} \lesssim 2000 \omega_{pe}^{-1}$  for slow electron holes. Panel (c) shows that typically we have  $0.5 \omega_{ce}^{-1} \lesssim \Delta t_{\max} \lesssim 20 \omega_{ce}^{-1}$  for fast electron holes and  $10 \omega_{ce}^{-1} \lesssim \Delta t_{\max} \lesssim 200 \omega_{ce}^{-1}$  for slow electron holes. We stress that  $\Delta t_{\max}$  is only a lower bound for electron hole lifetimes. A more detailed analysis of the lifetime of electron holes requires a spatial separation between the MMS spacecraft larger than a few tens of kilometers, which is typical for events in this study. Nevertheless, due to relatively small propagation velocities of slow electron holes we have been able to demonstrate that electron hole lifetimes can be at least a few thousands of  $\omega_{pe}^{-1}$  and a few hundred of  $\omega_{ce}^{-1}$ .

## 5. Discussion

### 5.1. Parameters and Origin of Electron Holes

We have found that electron holes in the Earth's magnetotail have distinctly different velocities from a few km/s, which is much smaller than typical ion thermal velocity, up to 20,000 km/s, which is comparable to typical electron thermal velocity. This statistical study confirms and extends the previous case studies, which reported the presence of electron holes with velocities of a few hundred and a few thousand km/s in the Earth's magnetotail (Cattell et al., 2005; Khotyaintsev et al., 2010; Norgren et al., 2015). Noteworthy that electron holes with distinctly different velocities were previously reported in reconnection current sheets at the magnetopause (Cattell et al., 2002; Graham et al., 2015, 2016). The origin of electron holes with distinctly different velocities has been recently discussed by Norgren, André, Graham, et al. (2015), who presented a linear stability analysis of electrostatic fluctuations in a plasma consisting of background ion and electron populations and a cold electron beam. In that stability analysis the density and velocity of the electron beam were varied in a wide range, so that the analysis covered the instabilities of bump-on-tail type (relatively tenuous beam with sufficiently large velocity) and Buneman type (sufficiently dense beam with relatively low velocity). Norgren, André, Graham, et al. (2015) showed that the bump-on-tail type instabilities produce electrostatic waves with relatively high phase velocity,  $\omega/k \gtrsim 0.1 V_{bg}$ , while the Buneman type instabilities produce electrostatic waves with relatively low phase velocity,  $\omega/k \lesssim 0.05 V_{bg}$ , where  $V_{bg}$  in the thermal velocity of the background electron population. In section 3 the separation of the data set into slow,

medium and fast electron holes using the thresholds of  $0.05 V_{Te}$  and  $0.1 V_{Te}$  for the electron hole velocity  $|V_{ESW} - V_{i||}|$  was motivated by the analysis of Norgren, André, Graham, et al. (2015). Another type of instability capable of producing slow electron holes is the warm bistream instability, which involves a couple of counterstreaming warm electron beams (Graham et al., 2016; Morse & Nielson, 1969a; Omura et al., 1996). In this section we delve into the origin and discussion of parameters of electron holes in the Earth's magnetotail.

The analysis in Figures 2 and 3 showed that the electron holes are Debye-scale structures with typical parallel spatial scales  $\lambda_D \lesssim d_{||} \lesssim 10 \lambda_D$  and amplitudes  $10^{-3} T_e \lesssim e\Phi_0 \lesssim 0.1 T_e$ . The parallel spatial scales of a few Debye lengths and a positive correlation between  $d_{||}$  and  $\lambda_D$  are explained by the fact that the fastest growing electrostatic fluctuations driven by electron streaming instabilities have wavelengths from a few up to a few tens of Debye lengths (e.g., Buneman, 1959; Graham et al., 2016; Norgren, André, Graham, et al., 2015; Omura et al., 1996). The typical parallel spatial scales  $\lambda_D \lesssim d_{||} \lesssim 10 \lambda_D$  and a positive correlation between  $d_{||}$  and  $\lambda_D$  were previously reported for electron holes observed in the inner magnetosphere, auroral region and reconnection current sheets (Cattell et al., 2002, 2003; Ergun et al., 1999; Franz et al., 2005; Graham et al., 2016).

The observed electron hole parameters allow rough estimates of growth rates of instabilities seeding formation of the electron holes. An electron streaming instability seeding formation of electron holes saturates, when the amplitude of electrostatic fluctuations is sufficiently large, so that the bounce frequency of electrons trapped by the electrostatic fluctuations is comparable to an initial growth rate  $\gamma$  of the instability (Drummond et al., 1970; Manheimer, 1971; Mizuno & Tanaka, 1972; Sagdeev & Galeev, 1969). Therefore, the bounce frequency of electrons trapped by bipolar parallel electric fields of electron holes,  $\omega_{be} = d_{||}^{-1} (e\Phi_0/m_e)^{1/2}$ , is expected to be of the order of the initial growth rate  $\gamma$ , which can be written in the form of the estimate of electron hole amplitude

$$e\Phi_0 \sim m_e \gamma^2 d_{||}^2 \quad (2)$$

There are several critical comments to be done on the estimate  $\omega_{be} \sim \gamma$ . First, this estimate is accurate only up to a numerical factor between 1 and 10 (Dewar, 1973). Second, strictly speaking this estimate is valid for electrostatic fluctuations after being saturated, but before isolated electron holes are formed due to the merging of phase space vortexes of electrons trapped by those electrostatic fluctuations (see Morse & Nielson, 1969b; Roberts & Berk, 1967; Saeki et al., 1979, for early simulations and measurements of the merging process). There is currently absent a detailed analysis of effects of the merging process on the saturated amplitude of electron holes, but we expect that the estimate  $\omega_{be} \sim \gamma$  is correct at least by the order of magnitude. Third and most critical, the estimate  $\omega_{be} \sim \gamma$  is valid only for instabilities driven by resonant electrons (e.g., bump-on-tail instability), but strongly underestimates saturated amplitudes, for example, of the classical Buneman instability, because ions critically affect the nonlinear evolution of the instability (see, e.g., simulations by Büchner & Elkina, 2006; Che et al., 2013; Jara-Almonte et al., 2014). The ion dynamics can also critically affect the saturation of warm bistream instabilities, because unstable electrostatic waves may have velocities comparable to the ion thermal velocity (e.g., Graham et al., 2016; Morse & Nielson, 1969a). To the best of our knowledge, there is currently absent a through analysis of saturated amplitudes of Buneman type and warm bistream instabilities capable of producing slow electron holes (Graham et al., 2016; Norgren et al., 2015), but the criterion  $\omega_{be} \sim \gamma$  is expected to provide at least a lower bound for saturated amplitudes of these instabilities (e.g., Büchner & Elkina, 2006; Jara-Almonte et al., 2014).

Keeping in mind these caveats, we will use Equation 2 for order of magnitude estimates of electron hole amplitudes. Equation 2 shows that the growth rate can be estimated as follows

$$\frac{\gamma}{\omega_{pe}} \sim \left( \frac{e\Phi_0}{T_e} \right)^{1/2} \frac{\lambda_D}{d_{||}} \quad (3)$$

The electron hole parameters in Figure 2c indicate that the growth rates should be in the range  $\gamma/\omega_{pe} \sim 0.01 - 0.1$ . For reasons mentioned above, for slow electron holes, potentially produced by Buneman type

and warm bistream instabilities, it is more accurate to state that  $\gamma/\omega_{pe} \lesssim 0.01 - 0.1$ . In any case, these growth rates are consistent with those expected for electron bump-on-tail, warm bistream and Buneman-type instabilities at typical parameters in the Earth's magnetotail (see, e.g., linear stability analyses by Graham et al., 2016; Norgren, André, Graham, et al., 2015). For electron density of  $0.1 \text{ cm}^{-3}$  that is typical of the Earth's magnetotail (supporting information), the inverse growth rate is  $\gamma^{-1} \sim 1-10 \text{ ms}$ , indicating thereby that the saturation of the instabilities seeding the formation of electron holes occurs on a time scale of a few milliseconds. Therefore, the electron velocity distribution functions measured by the MMS plasma instrument during electron hole observations are expected to correspond to a marginally stable saturated state. The analysis of electron hole parameters provides then a valuable diagnostic of instabilities operating on time scales not resolvable by plasma instruments.

The analysis in Figure 3 demonstrated the positive correlation between  $d_{||}$  and  $2\pi|V_{ESW} - V_{i||}|/\omega_{pe}$  for the fast electron holes, i.e.  $|V_{ESW} - V_{i||}| > 0.1 V_{Te}$ . This correlation indicates that fast electron holes are highly likely produced by a bump-on-tail instability. For the bump-on-tail instability the phase velocity of the fastest growing electrostatic waves should be correlated with electron beam velocity  $V_b$ , the frequency  $\omega_0$  of these waves should be a fraction of the electron plasma frequency  $\omega_{pe}$  and, hence, the wavelength should be  $\lambda_0 \approx 2\pi V_b/\omega_{pe} \cdot (\omega_{pe}/\omega_0)$  (e.g., Omura et al., 1996; Umeda et al., 2004). Therefore, for electron holes seeded by the bump-on-tail instability we expect to have  $d_{||}$  correlated with  $2\pi|V_{ESW} - V_{i||}|/\omega_{pe}$ , because  $d_{||}$  should be correlated with  $\lambda_0$  and  $|V_{ESW} - V_{i||}|$  should be correlated with  $V_b$ . Moreover, assuming that  $d_{||}$  is comparable to  $\lambda_0 \approx 2\pi V_b/\omega_{pe} \cdot (\omega_{pe}/\omega_0)$  we expect  $d_{||}$  to be a few times larger than  $2\pi|V_{ESW} - V_{i||}|/\omega_{pe}$ , which is indeed consistent with the experimental data in Figure 3b.

The absence of a correlation between  $d_{||}$  and  $2\pi|V_{ESW} - V_{i||}|/\omega_{pe}$  for the slow electron holes indicates that the majority of them cannot be produced by the classical Buneman instability. The classical Buneman instability drives electrostatic waves satisfying the dispersion relation  $\omega = kV_b \cdot 2^{-4/3} (m_e/m_i)^{1/3} \approx 0.03 \cdot kV_b$  and the fastest growing waves have wavelength  $\lambda_0 \approx 2\pi V_b/\omega_{pe}$ , where  $V_b$  is the bulk velocity of the electron population, which should be comparable to the electron thermal velocity (Buneman, 1959; Mikhailovskii, 1974). The velocity of electron holes seeded by the Buneman instability is expected to be  $|V_{ESW} - V_{i||}| \approx 0.03 V_b$ , while the parallel spatial scales  $d_{||}$  are expected to be comparable to  $\lambda_0$ . Therefore, the spatial scales of electron holes seeded by the classical Buneman instability should be correlated with the electron hole velocities,  $d_{||} \approx 30 \cdot 2\pi|V_{ESW} - V_{i||}|/\omega_{pe}$ . The visual inspection of Figure 3 shows that the relation  $d_{||} \approx 30 \cdot 2\pi|V_{ESW} - V_{i||}|/\omega_{pe}$  relatively well describes the spatial scales of the slow electron holes by the order of magnitude, but the absence of a distinct correlation between  $d_{||}$  and  $2\pi|V_{ESW} - V_{i||}|/\omega_{pe}$  is an argument against the classical Buneman instability as the source of the majority of the slow electron holes. Although the classical Buneman instability is not likely to produce the slow electron holes (in a statistical sense), we cannot rule out that the slow electron holes are seeded by Buneman type instabilities suggested by Norgren, André, Graham, et al. (2015). The analysis of linear stability predictions and nonlinear evolution of Buneman type instabilities deserve a dedicated study.

The observed properties of slow electron holes do not contradict to linear stability predictions of warm electron bistream instabilities. In the case of identical counterstreaming electron beams, the electron bistream instability produces purely growing electrostatic fluctuations with zero phase velocity in the plasma rest frame and typical wavelength  $\lambda_0 \approx 2\pi V_b/\omega_{pe}$ , where  $V_b$  and  $-V_b$  are electron beam velocities (Goldman et al., 1999; Mikhailovskii, 1974; Morse & Nielson, 1969a). Therefore, in the case of identical electron beams there is expected no correlation between the spatial scales and velocities of electron holes seeded by the electron bistream instability. In realistic situations the electron beams are certainly not identical, but this cannot result in a correlation between the parallel spatial scale and velocity of electron holes, because the velocity of the fastest growing waves is determined by the asymmetry between densities and velocities of the beams, while the spatial scales are determined by the beam velocities.

Thus, fast electron holes are most likely produced by bump-on-tail instabilities, while slow electron holes can be, in principle, produced by warm bistream instabilities, but Buneman type instabilities cannot be ruled out. According to numerical simulations by Che et al. (2009, 2010) slow and fast electron holes may coexist in reconnection current sheets, where slow electron holes are produced by the Buneman instability, while fast electron holes are produced by low-hybrid or two-stream instabilities after saturation of the Buneman

instability. In section 4 we have presented statistical distributions of time intervals between sequentially observed fast and slow electron holes and demonstrated that the time interval between the different types of electron holes is typically larger than 10 seconds. We conclude that in a statistical sense fast and slow electron holes in the Earth's magnetotail are not associated with each other. We note though, that simulations by Che et al. (2009, 2010) predict coexistence of fast and slow electron holes in reconnection regions, which statistical weight in our data set is probably negligible, because reconnection regions are rather localized in space and time

A few more comments are in order on the origin of electron holes in the Earth's magnetotail. First, we have addressed a relation between the amplitudes of  $E_{\parallel}$  of the electron holes and a local current density estimated by the curlometer technique as well as a local electron temperature. In both cases we have found no definite correlation between these quantities (not shown here). Second, the recent measurements in the inner magnetosphere showed that electrostatic solitary waves can be associated and phase correlated with whistler waves (Agapitov et al., 2018; An et al., 2019; Malaspina et al., 2018; Vasko, Agapitov, Mozer, et al., 2018). We have inspected electric and magnetic field waveforms measured over 100 ms around each of 2,426 electron holes and could not identify any whistler waves associated and phase correlated with the electron holes. Thus, electron holes around fast plasma flows in the Earth's magnetotail are statistically produced by electron streaming instabilities rather than by nonlinear processes associated with whistler waves.

### 5.2. Velocity Gap

The normalization of electron holes velocities in the plasma rest frame to a local ion thermal velocity  $V_{Ti}$  revealed the presence of the gap in the distribution of electron hole velocities at  $V_{Ti} \lesssim |V_{ESW} - V_{i\parallel}| \lesssim 2 V_{Ti}$ . There are the following interpretations of this velocity gap. First, Vlasov simulations by Zhou and Hutchinson (2018) have recently shown that electron holes with velocities slightly above the ion-acoustic velocity  $c_s$  are self-accelerated due to interaction with ions to velocities above about  $2 c_s$ . According to Zhou and Hutchinson (2018) there should be a gap between about  $c_s$  and  $2 c_s$  in the distribution of electron holes velocities. At velocities below  $c_s$  an electron hole represent a coupled state of electron hole and ion-acoustic soliton (see also Tran, 1979, for review), while above about  $2c_s$  electron holes are in effect not affected by ions. The Vlasov simulations by Zhou and Hutchinson (2018) were initialized with already formed electron hole in a plasma with  $T_e \gg T_i$ , so that  $c_s = [(T_e + \gamma_i T_i)/m_i]^{1/2}$ , where  $\gamma_i = 3$  is the ion polytropic index at  $c_s \gg V_{Ti}$  (e.g., Mikhailovskii, 1974). On the other hand, for the majority of the electron holes in the Earth's magnetotail we have  $T_i \gg T_e$  (Figure 2a), so that ion-acoustic waves are strongly damped in this regime (e.g., Mikhailovskii, 1974), because  $c_s$  is comparable to the ion thermal velocity  $V_{Ti}$  (note that at  $c_s$  comparable to  $V_{Ti}$  we have  $\gamma_i$  of the order of 1, but  $\gamma_i \neq 3$ ). Provided the simulation results of Zhou and Hutchinson (2018) are valid at  $T_i \gg T_e$ , we would expect the velocity gap around the ion thermal velocity in accordance with experimental data in Figure 4.

The alternative/additional interpretation is that electron holes with velocities around a local ion thermal velocity are not observed, because (a) electrostatic fluctuations with phase velocity around  $V_{Ti}$  are stable in the linear regime due to the ion Landau damping or (b) electron holes, which were originally produced with velocities different from  $V_{Ti}$ , but evolved toward  $V_{Ti}$  due to propagation in a nonuniform plasma are Landau damped by ions (see Briand et al., 2008; Kuzichev et al., 2017; Mandrake et al., 2000; Vasko, Kuzichev, et al., 2017, for simulations of electron hole evolution in nonuniform plasmas). Whether electron holes can be indeed damped by ions in Scenario (b) certainly depends on the relation between the ion Landau damping rate and acceleration/deceleration rate of electron holes in a nonuniform plasma. The detailed analysis of both alternative/additional scenarios deserves a dedicated study.

### 5.3. Lifetime, Transverse Instability, and Its Implications

The analysis in Figure 5 demonstrated that independent of velocity, the electron hole parameters are below the transverse instability threshold, i.e.  $\omega_{be} \lesssim Y \omega_{ce}$ , with  $Y = 1.5$  providing reasonable agreement with observations. The electron holes observed at  $\omega_{pe}/\omega_{ce} > 10$  can be around the transverse instability threshold, in contrast to the electron holes observed at  $\omega_{pe}/\omega_{ce} < 10$ . The reason for that critical role of  $\omega_{pe}/\omega_{ce}$  is explained as follows. The growth rates  $\gamma$  of electron streaming instabilities seeding the formation of electron holes is proportional to  $\omega_{pe}$ , and does not depend on  $\omega_{ce}$ , because the fastest growing electrostatic waves propagate parallel to a local magnetic field (e.g., Goldman et al., 2008; Miyake et al., 1998; Omura et al., 1996;

Umeda et al., 2006). At  $\gamma \lesssim Y\omega_{ce}$  the saturation occurs at amplitudes given by Equation 2, which is below the transverse instability threshold given by Equation 1. At  $\gamma \gtrsim Y\omega_{ce}$  electron hole amplitudes could be  $e\Phi_0 \sim m_e \gamma^2 d_{\parallel}^2$ , but the transverse instability keeps electron hole amplitudes at lower level,  $e\Phi_0 \sim Y^2 m_e \omega_{ce}^2 d_{\parallel}^2$ . Thus, we deduce the following upper threshold for electron hole amplitudes

$$e\Phi_0 \lesssim m_e \varpi^2 d_{\parallel}^2, \quad \varpi = \min(\gamma, Y\omega_{ce}) \quad (4)$$

At sufficiently large  $\omega_{pe}/\omega_{ce}$  the increment  $\gamma$ , being proportional to  $\omega_{pe}$ , can be larger than  $Y\omega_{ce}$  and in that case the amplitudes of electron holes are controlled by the transverse instability. On the other hand, at sufficiently small  $\omega_{pe}/\omega_{ce}$  the initial growth rate is less likely to be larger than  $Y\omega_{ce}$  and electron holes saturate at amplitudes well below the transverse instability threshold, so that the transverse instability is not involved in the control of electron hole amplitudes.

We note that the transverse instability can be involved into the electron hole dynamics provided that electron hole lifetime is longer than  $\omega_{ce}^{-1}$ . In section 4 we have demonstrated that the lifetime of the majority of the electron holes is indeed larger than  $\omega_{ce}^{-1}$  (Figure 8). In principle, there can be electron holes in the space plasma, which are formed and dissipated on time scales less than  $\omega_{ce}^{-1}$  that is before the transverse instability has a chance to develop. The dynamics and parameters of these electron holes cannot be controlled by the transverse instability. The lifetime of such electron holes in the Earth's magnetotail should be rather short though, because  $\omega_{ce}^{-1}$  is only about 1 ms at typical background magnetic field of 10 nT.

There are several valuable implications of the transverse instability criterion for future studies of electrostatic solitary waves in various space plasma environments. The transverse instability criterion can be used to infer the nature of solitary waves in plasma environments, where spacecraft measurements are limited. For example, spacecraft measurements in the solar wind do not generally allow estimating the velocity and, hence, inferring the nature of electrostatic solitary waves measured around current sheets (Malaspina et al., 2013; Mangeney et al., 1999) and interplanetary shock waves (Williams et al., 2005; Wilson III et al., 2007; Wilson et al., 2010). The transverse instability threshold allows testing a hypothesis that a solitary wave is electron phase space hole provided the lifetime of the solitary wave is known to be larger than  $\omega_{ce}^{-1}$  (the temporal width  $\tau_{pp}$  can be used as a lower bound of the lifetime of a solitary wave measured aboard a single spacecraft). The transverse instability threshold (1) can be written in the form of an upper estimate of the peak-to-peak amplitude  $E_{pp}$  of the bipolar parallel electric field

$$\frac{E_{pp}}{B_0} \lesssim 2 V_{Te} \frac{\omega_{ce} d_{\parallel}}{\omega_{pe} \lambda_D}, \quad (5)$$

where  $B_0$  is the background magnetic field,  $V_{Te} = (2T_e/m_e)^{1/2}$  is the electron thermal velocity. In derivation of Equation 5 we have assumed  $Y = 1.5$  and that the solitary wave can be described by the Gaussian model,  $\Phi = \Phi_0 \exp(-z^2/2d_{\parallel}^2)$ , so that  $\Phi_0 = 0.5E_{pp}d_{\parallel} \exp(0.5)$ .

The presented analysis along with previous measurements at the magnetopause and in the inner magnetosphere showed that electron holes typically have  $1 \lesssim d_{\parallel}/\lambda_D \lesssim 10$  (e.g., Ergun et al., 1999; Franz et al., 2005; Graham et al., 2016). Therefore, solitary waves measured aboard a single spacecraft and satisfying Equation 5 with  $d_{\parallel} = 10\lambda_D$  can be, in principle, electron holes and the expected range of velocities in the spacecraft frame is  $2\lambda_D/\tau_{pp} \lesssim V_{ESW} \lesssim 20\lambda_D/\tau_{pp}$ . We should note though that Equation 5 is only a necessary, but not sufficient, condition for a solitary wave to be interpreted in terms of electron holes. In other words, solitary waves strongly violating Equation 5 with  $d_{\parallel} = 10\lambda_D$  are highly unlikely to be electron holes. In that case these solitary waves are more likely to be ion holes, indicating thereby a potential operation of ion streaming instabilities in a considered plasma environment. One could argue that according to the transverse instability criterion given by Equation 1, but with electron parameters replaced by ion parameters, ion holes should actually saturate at even lower amplitudes than electron holes. However, the fundamental difference of ion holes from electron holes is that the inverse ion gyrofrequency  $\omega_{ci}^{-1}$  is a much longer period of time than  $\omega_{ce}^{-1}$  (at 10 nT background magnetic field  $\omega_{ci}^{-1}$  is about 1 second) and, hence, ion holes can be produced and dissipated well before the transverse instability has a



chance to develop. That is the case, for example, in the Earth's bow shock, where solitary waves measured aboard Wind spacecraft and originally interpreted in terms of electron holes (Bale et al., 1998, 2002), though they strongly violated the estimate given by Equation 5, finally turned out to be ion holes as revealed by Cluster (Hobara et al., 2008) and MMS measurements (Vasko, Mozer, Krasnoselskikh, et al., 2018; Vasko et al., 2020; Wang et al., 2020).

The other valuable application of the transverse instability criterion is that it allows estimating parameters of electron holes, which lifetime is longer than  $\omega_{ce}^{-1}$ , potentially present in plasma environments, where in situ measurements are not available. For example, Equation 4 can be used to estimate the amplitude of electron holes in astrophysical collisionless shocks, which is a valuable information, because according to numerical simulations electron holes might be involved into electron acceleration in high-Mach number collisionless shocks (Hoshino & Shimada, 2002; Schmitz et al., 2002).

## 6. Conclusions

We have addressed origin, parameters and transverse instability of electron phase space holes in the Earth's magnetotail using a unique data set of more than 8,300 electrostatic solitary waves measured aboard MMS1 and more than 2,400 of these solitary waves measured aboard several MMS spacecraft and interpreted in terms of electron phase space holes. The multispacecraft interferometry allowed us to address electron hole properties in a wide range of electron hole velocities. The major results of the statistical analysis can be summarized as follows:

1. Electron holes have distinctly different velocities in the plasma rest frame,  $|V_{ESW} - V_{i||}|$  is in the range from just a few km/s up to 20,000 km/s, electrostatic potential amplitudes  $\Phi_0$  are from a few up to a few hundred volts and parallel spatial scales  $d_{i||}$  are from 0.5 up to 30 km. In normalized units the spatial scales and amplitudes are typically  $\lambda_D \lesssim d_{i||} \lesssim 10 \lambda_D$  and  $10^{-3} T_e \lesssim e\Phi_0 \lesssim 0.1 T_e$ . The parallel spatial scales are shown to be correlated with a local Debye length  $\lambda_D$ .
2. The comparison between  $d_{i||}$  and  $2\pi|V_{ESW} - V_{i||}|/\omega_{pe}$  revealed that fast electron holes (velocities in the plasma rest frame satisfy  $|V_{ESW} - V_{i||}| \gtrsim 0.1 V_{Te}$ ) are highly likely produced by the bump-on-tail instability. The observed parameters of slow electron holes (velocities satisfy  $|V_{ESW} - V_{i||}| \lesssim 0.05 V_{Te}$ ) do not contradict the generation by warm bistream instabilities, and we cannot rule out Buneman type instabilities either.
3. There is a gap in the distribution of electron hole velocities around a local ion thermal velocity,  $V_{Ti} \lesssim |V_{ESW} - V_{i||}| \lesssim 2 V_{Ti}$ , where  $V_{Ti}$  is a local ion thermal velocity. The gap is suggested to be the evidence for self-acceleration process of electron holes recently reported in Vlasov simulations (Zhou & Hutchinson, 2018), while the alternative/additional interpretation is that electron holes with velocities around the local ion thermal velocity are damped via the ion Landau damping. The gap naturally separates slow electron holes with  $|V_{ESW} - V_{i||}| < 0.05 V_{Te}$  and fast electron holes with  $|V_{ESW} - V_{i||}| > 0.1 V_{Te}$  in the velocity space.
4. We have shown that electron hole parameters are below the transverse instability criterion,  $\omega_{be} \lesssim 1.5 \omega_{ce}$ , and provided arguments in favor that the nonlinear saturation criterion,  $\omega_{be} \sim \gamma$ , also restricts electron hole parameters. We have deduced the following upper estimate for electron hole amplitudes:  $e\Phi_0 \lesssim m_e \varpi^2 d_{i||}^2$ , where  $\varpi = \min(\gamma, 1.5 \omega_{ce})$ . The amplitudes of electron holes at  $\omega_{pe}/\omega_{ce} > 10$  are more likely to be controlled by the transverse instability than the amplitudes of electron holes at smaller  $\omega_{pe}/\omega_{ce}$ , because the increments  $\gamma$  of electron streaming instabilities are proportional to  $\omega_{pe}$ .
5. The analysis of temporal characteristics demonstrated that fast and slow electron holes in the Earth's magnetotail can be generally distinguished by the temporal peak-to-peak width of a bipolar  $E_{i||}$  signal. More than 95% of fast electron holes have  $\tau_{pp} < 3$  ms and more than 95% of slow electron holes have  $\tau_{pp} > 3$  ms.
6. The statistical analysis of time intervals between sequentially observed fast and slow electron holes showed that electron holes of the different types are not associated with each other and produced by instabilities, which operate independently.
7. The analysis of time delays between observations of the same electron hole aboard different MMS spacecraft allowed to obtain lower bounds for electron hole lifetimes. We showed that these lower bounds can

be as large as a few thousands of  $\omega_{pe}^{-1}$  and a few hundred of  $\omega_{ce}^{-1}$ , where  $\omega_{pe}$  and  $\omega_{ce}$  are electron plasma frequency and electron cyclotron frequency, respectively.

### Data Availability Statement

The data are publicly available online (at <https://lasp.colorado.edu/mms/sdc/public/>).

### Acknowledgments

The work was supported by NASA MMS Guest Investigator Grant 80NSSC18K0155 and NASA Grant 80NSSC19K1063. A. A. thanks the Russian Science Foundation for support through Grant 19-12-00313. I. V. is thankful for the support of the International Space Science Institute (ISSI), Bern, Switzerland. We thank the MMS teams for the excellent data.

### References

Agapitov, O., Drake, J. F., Vasko, I., Mozer, F. S., Artemyev, A., Krasnoselskikh, V., et al. (2018). Nonlinear electrostatic steepening of whistler waves: The guiding factors and dynamics in inhomogeneous systems. *Geophysical Research Letters*, *45*, 2168–2176. <https://doi.org/10.1002/2017GL076957>

An, X., Li, J., Bortnik, J., Decyk, V., Kletzing, C., & Hospodarsky, G. (2019). Unified view of nonlinear wave structures associated with whistler-mode chorus. *Physical Review Letters*, *122*(4), 045101. <https://doi.org/10.1103/PhysRevLett.122.045101>

Artemyev, A. V., Baumjohann, W., Petrukovich, A. A., Nakamura, R., Dandouras, I., & Fazakerley, A. (2011). Proton/electron temperature ratio in the magnetotail. *Annales Geophysicae*, *29*(12), 2253–2257. <https://doi.org/10.5194/angeo-29-2253-2011>

Artemyev, A. V., Rankin, R., & Vasko, I. Y. (2017). Nonlinear Landau resonance with localized wave pulses. *Journal of Geophysical Research: Space Physics*, *122*, 5519–5527. <https://doi.org/10.1002/2017JA024081>

Bale, S. D., Hull, A., Larson, D. E., Lin, R. P., Muschietti, L., Kellogg, P. J., et al. (2002). Electrostatic turbulence and Debye-scale structures associated with electron thermalization at collisionless shocks. *The Astrophysical Journal Letters*, *575*, L25–L28. <https://doi.org/10.1086/342609>

Bale, S. D., Kellogg, P. J., Larsen, D. E., Lin, R. P., Goetz, K., & Lepping, R. P. (1998). Bipolar electrostatic structures in the shock transition region: Evidence of electron phase space holes. *Geophysical Research Letters*, *25*, 2929–2932. <https://doi.org/10.1029/98GL02111>

Børve, S., Pécseli, H. L., & Trulsen, J. (2001). Ion phase-space vortices in 2.5-dimensional simulations. *Journal of Plasma Physics*, *65*(2), 107–129. <https://doi.org/10.1017/S0022377801008947>

Bounds, S. R., Pfaff, R. F., Knowlton, S. F., Mozer, F. S., Temerin, M. A., & Kletzing, C. A. (1999). Solitary potential structures associated with ion and electron beams near 1r<sub>E</sub> altitude. *Journal of Geophysical Research*, *104*(A12), 28,709–28,718. <https://doi.org/10.1029/1999JA900284>

Briand, C., Mangeney, A., & Califano, F. (2008). Coherent electric structures: Vlasov-Ampère simulations and observational consequences. *Journal of Geophysical Research*, *113*, A07219. <https://doi.org/10.1029/2007JA012992>

Büchner, J., & Elkina, N. (2006). Anomalous resistivity of current-driven isothermal plasmas due to phase space structuring. *Physics of Plasmas*, *13*(8), 082304. <https://doi.org/10.1063/1.2209611>

Buneman, O. (1959). Dissipation of currents in ionized media. *Physical Review*, *115*, 503–517. <https://doi.org/10.1103/PhysRev.115.503>

Burch, J. L., Moore, T. E., Torbert, R. B., & Giles, B. L. (2016). Magnetospheric Multiscale overview and science objectives. *Space Science Reviews*, *199*(1–4), 5–21. <https://doi.org/10.1007/s11214-015-0164-9>

Cattell, C., Crumley, J., Dombeck, J., Wygant, J. R., & Mozer, F. S. (2002). Polar observations of solitary waves at the Earth's magnetopause. *Geophysical Research Letters*, *29*, 1065. <https://doi.org/10.1029/2001GL014046>

Cattell, C., Dombeck, J., Wygant, J., Drake, J. F., Swisdak, M., Goldstein, M. L., et al. (2005). Cluster observations of electron holes in association with magnetotail reconnection and comparison to simulations. *Journal of Geophysical Research*, *110*, A01211. <https://doi.org/10.1029/2004JA010519>

Cattell, C., Neiman, C., Dombeck, J., Crumley, J., Wygant, J., Kletzing, C. A., et al. (2003). Large amplitude solitary waves in and near the Earth's magnetosphere, magnetopause and bow shock: Polar and Cluster observations. *Nonlinear Processes in Geophysics*, *10*, 13–26.

Che, H., Drake, J. F., Swisdak, M., & Goldstein, M. L. (2013). The adiabatic phase mixing and heating of electrons in Buneman turbulence. *Physics of Plasmas*, *20*(6), 061205. <https://doi.org/10.1063/1.4811137>

Che, H., Drake, J. F., Swisdak, M., & Yoon, P. H. (2009). Nonlinear development of streaming instabilities in strongly magnetized plasma. *Physical Review Letters*, *102*(14), 145004. <https://doi.org/10.1103/PhysRevLett.102.145004>

Che, H., Drake, J. F., Swisdak, M., & Yoon, P. H. (2010). Electron holes and heating in the reconnection dissipation region. *Geophysical Research Letters*, *37*, L11105. <https://doi.org/10.1029/2010GL043608>

Deng, X., Ashour-Abdalla, M., Zhou, M., Walker, R., El-Alaoui, M., Angelopoulos, V., et al. (2010). Wave and particle characteristics of earthward electron injections associated with dipolarization fronts. *Journal of Geophysical Research*, *115*, A09225. <https://doi.org/10.1029/2009JA015107>

Dewar, R. L. (1973). Saturation of kinetic plasma instabilities by particle trapping. *Physics of Fluids*, *16*(3), 431–435. <https://doi.org/10.1063/1.1694358>

Drake, J. F., Swisdak, M., Cattell, C., Shay, M. A., Rogers, B. N., & Zeiler, A. (2003). Formation of electron holes and particle energization during magnetic reconnection. *Science*, *299*, 873–877. <https://doi.org/10.1126/science.1080333>

Drummond, W. E., Malmberg, J. H., O'Neil, T. M., & Thompson, J. R. (1970). Nonlinear development of the beam-plasma instability. *Physics of Fluids*, *13*(9), 2422–2425. <https://doi.org/10.1063/1.1693255>

Dupree, T. H. (1982). Theory of phase-space density holes. *Physics of Fluids*, *25*(2), 277–289. <https://doi.org/10.1063/1.863734>

Ergun, R. E., Carlson, C. W., McFadden, J. P., Mozer, F. S., Muschietti, L., Roth, I., & Strangeway, R. J. (1998). Debye-scale plasma structures associated with magnetic-field-aligned electric fields. *Physical Review Letters*, *81*, 826–829. <https://doi.org/10.1103/PhysRevLett.81.826>

Ergun, R. E., Carlson, C. W., Muschietti, L., Roth, I., & McFadden, J. P. (1999). Properties of fast solitary structures. *Nonlinear Processes in Geophysics*, *6*, 187–194.

Ergun, R. E., Goodrich, K. A., Stawarz, J. E., Andersson, L., & Angelopoulos, V. (2015). Large-amplitude electric fields associated with bursty bulk flow braking in the Earth's plasma sheet. *Journal of Geophysical Research: Space Physics*, *120*, 1832–1844. <https://doi.org/10.1002/2014JA020165>

Ergun, R. E., Tucker, S., Westfall, J., Goodrich, K. A., Malaspina, D. M., Summers, D., et al. (2016). The axial double probe and fields signal processing for the MMS mission. *Space Science Reviews*, *199*, 167–188. <https://doi.org/10.1007/s11214-014-0115-x>

Fox, W., Porkolab, M., Egedal, J., Katz, N., & Le, A. (2008). Laboratory observation of electron phase-space holes during magnetic reconnection. *Physical Review Letters*, *101*(25), 255003. <https://doi.org/10.1103/PhysRevLett.101.255003>

- Franz, J. R., Kintner, P. M., Pickett, J. S., & Chen, L.-J. (2005). Properties of small-amplitude electron phase-space holes observed by polar. *Journal of Geophysical Research*, *110*, A09212. <https://doi.org/10.1029/2005JA011095>
- Franz, J. R., Kintner, P. M., Seyler, C. E., Pickett, J. S., & Scudder, J. D. (2000). On the perpendicular scale of electron phase-space holes. *Geophysical Research Letters*, *27*, 169–172. <https://doi.org/10.1029/1999GL010733>
- Goldman, M. V., Newman, D. L., Lapenta, G., Andersson, L., Gosling, J. T., Eriksson, S., et al. (2014). Čerenkov emission of quasiparallel whistlers by fast electron phase-space holes during magnetic reconnection. *Physical Review Letters*, *112*(14), 145002. <https://doi.org/10.1103/PhysRevLett.112.145002>
- Goldman, M. V., Newman, D. L., & Pritchett, P. (2008). Vlasov simulations of electron holes driven by particle distributions from PIC reconnection simulations with a guide field. *Geophysical Research Letters*, *35*, L22109. <https://doi.org/10.1029/2008GL035608>
- Goldman, M. V., Oppenheim, M. M., & Newman, D. L. (1999). Nonlinear two-stream instabilities as an explanation for auroral bipolar wave structures. *Geophysical Research Letters*, *26*, 1821–1824. <https://doi.org/10.1029/1999GL900435>
- Graham, D. B., Khotyaintsev, Y. V., Vaivads, A., & André, M. (2015). Electrostatic solitary waves with distinct speeds associated with asymmetric reconnection. *Geophysical Research Letters*, *42*, 215–224. <https://doi.org/10.1002/2014GL02538>
- Graham, D. B., Khotyaintsev, Y. V., Vaivads, A., & André, M. (2016). Electrostatic solitary waves and electrostatic waves at the magnetopause. *Journal of Geophysical Research: Space Physics*, *121*, 3069–3092. <https://doi.org/10.1002/2015JA021527>
- Gurevich, A. V. (1968). Distribution of captured particles in a potential well in the absence of collisions. *Soviet Journal of Experimental and Theoretical Physics*, *26*, 575.
- Gurnett, D. A., Frank, L. A., & Lepping, R. P. (1976). Plasma waves in the distant magnetotail. *Journal of Geophysical Research*, *81*, 6059–6071. <https://doi.org/10.1029/JA081i034p06059>
- Hobara, Y., Walker, S. N., Balikhin, M., Pokhotelov, O. A., Gedalin, M., Krasnoselskikh, V., et al. (2008). Cluster observations of electrostatic solitary waves near the Earth's bow shock. *Journal of Geophysical Research*, *113*, A05211. <https://doi.org/10.1029/2007JA012789>
- Holmes, J. C., Ergun, R. E., Newman, D. L., Ahmadi, N., Andersson, L., Le Contel, O., et al. (2018). Electron phase-space holes in three dimensions: Multispacecraft observations by Magnetospheric Multiscale. *Journal of Geophysical Research: Space Physics*, *123*, 9963–9978. <https://doi.org/10.1029/2018JA025750>
- Hoshino, M., & Shimada, N. (2002). Nonthermal electrons at high Mach number shocks: Electron shock surfing acceleration. *The Astrophysical Journal*, *572*(2), 880–887. <https://doi.org/10.1086/340454>
- Huang, C., Lu, Q., Wang, P., Wu, M., & Wang, S. (2014). Characteristics of electron holes generated in the separatrix region during antiparallel magnetic reconnection. *Journal of Geophysical Research: Space Physics*, *119*, 6445–6454. <https://doi.org/10.1002/2014JA019991>
- Hutchinson, I. H. (2017). Electron holes in phase space: What they are and why they matter. *Physics of Plasmas*, *24*(5), 055601. <https://doi.org/10.1063/1.4976854>
- Hutchinson, I. H. (2018). Kinematic mechanism of plasma electron hole transverse instability. *Physical Review Letters*, *205101*(20). <https://doi.org/10.1103/PhysRevLett.120.205101>
- Hutchinson, I. H. (2019). Transverse instability magnetic field thresholds of electron phase-space holes. *Physical Review E*, *99*(5), 053209. <https://doi.org/10.1103/PhysRevE.99.053209>
- Jara-Almonte, J., Daughton, W., & Ji, H. (2014). Debye scale turbulence within the electron diffusion layer during magnetic reconnection. *Physics of Plasmas*, *21*(3), 032114. <https://doi.org/10.1063/1.4867868>
- Khotyaintsev, Y. V., Graham, D. B., Steinvall, K., Alm, L., Vaivads, A., Johlander, A., et al. (2020). Electron heating by Debye-scale turbulence in guide-field reconnection. *Physical Review Letters*, *124*(4), 045101. <https://doi.org/10.1103/PhysRevLett.124.045101>
- Khotyaintsev, Y. V., Vaivads, A., André, M., Fujimoto, M., Retinò, A., & Owen, C. J. (2010). Observations of slow electron holes at a magnetic reconnection site. *Physical Review Letters*, *105*(16), 165002. <https://doi.org/10.1103/PhysRevLett.105.165002>
- Kovalenko, V. P. (1983). Electron bunches in nonlinear collective beam-plasma interaction. *Soviet Physics Uspekhi*, *26*, 116–137. <https://doi.org/10.1070/PU1983v026n02ABEH004321>
- Krasovsky, V. L., Matsumoto, H., & Omura, Y. (1997). Bernstein-Greene-Kruskal analysis of electrostatic solitary waves observed with Geotail. *Journal of Geophysical Research*, *102*, 22,131–22,140. <https://doi.org/10.1029/97JA02033>
- Kuzichev, I. V., Vasko, I. Y., Agapitov, O. V., Mozer, F. S., & Artemyev, A. V. (2017). Evolution of electron phase space holes in inhomogeneous magnetic fields. *Geophysical Research Letters*, *44*, 2105–2112. <https://doi.org/10.1002/2017GL072536>
- Lakhina, G. S., Tsurutani, B. T., Kojima, H., & Matsumoto, H. (2000). “Broadband” plasma waves in the boundary layers. *Journal of Geophysical Research*, *105*, 27,791–27,832. <https://doi.org/10.1029/2000JA900054>
- Lapenta, G., Markidis, S., Divin, A., Goldman, M. V., & Newman, D. L. (2011). Bipolar electric field signatures of reconnection separatrices for a hydrogen plasma at realistic guide fields. *Geophysical Research Letters*, *38*, L17104. <https://doi.org/10.1029/2011GL048572>
- Le Contel, O., Nakamura, R., Breuillard, H., Argall, M. R., Graham, D. B., Fischer, D., et al. (2017). Lower hybrid drift waves and electromagnetic electron space-phase holes associated with dipolarization fronts and field-aligned currents observed by the Magnetospheric Multiscale mission during a substorm. *Journal of Geophysical Research: Space Physics*, *122*, 12,236–12,257. <https://doi.org/10.1002/2017JA024550>
- Lefebvre, B., Chen, L.-J., Gekelman, W., Kintner, P., Pickett, J., Pribyl, P., et al. (2010). Laboratory measurements of electrostatic solitary structures generated by beam injection. *Physical Review Letters*, *105*(11), 115001. <https://doi.org/10.1103/PhysRevLett.105.115001>
- Lindqvist, P.-A., Olsson, G., Torbert, R. B., King, B., Granoff, M., Rau, D., et al. (2016). The spin-plane double probe electric field instrument for MMS. *Space Science Reviews*, *199*, 137–165. <https://doi.org/10.1007/s11214-014-0116-9>
- Malaspina, D. M., Andersson, L., Ergun, R. E., Wygant, J. R., Bonnell, J. W., Kletzing, C., et al. (2014). Nonlinear electric field structures in the inner magnetosphere. *Geophysical Research Letters*, *41*, 5693–5701. <https://doi.org/10.1002/2014GL02538>
- Malaspina, D. M., & Hutchinson, I. H. (2019). Properties of electron phase space holes in the lunar plasma environment. *Journal of Geophysical Research: Space Physics*, *124*, 4994–5008. <https://doi.org/10.1029/2019JA026857>
- Malaspina, D. M., Newman, D. L., Willson III, L. B., Kellogg, P. J., & Kersten, K. (2013). Electrostatic solitary waves in the solar wind: Evidence for instability at solar wind current sheets. *Journal of Geophysical Research: Space Physics*, *118*, 591–599. <https://doi.org/10.1002/jgra.50102>
- Malaspina, D. M., Ukhorskiy, A., Chu, X., & Wygant, J. (2018). A census of plasma waves and structures associated with an injection front in the inner magnetosphere. *Journal of Geophysical Research: Space Physics*, *123*, 2566–2587. <https://doi.org/10.1002/2017JA025005>
- Mandrake, L., Pritchett, P. L., & Coroniti, F. V. (2000). Electron beam generated solitary structures in a nonuniform plasma system. *Geophysical Research Letters*, *27*, 2869–2872. <https://doi.org/10.1029/2000GL003785>
- Mangenev, A., Salem, C., Lacombe, C., Bougeret, J.-L., Perche, C., Manning, R., et al. (1999). WIND observations Of coherent electrostatic waves in the solar wind. *Annales Geophysicae*, *17*, 307–320. <https://doi.org/10.1007/s00585-999-0307-y>

- Manheimer, W. M. (1971). Strong turbulence theory of nonlinear stabilization and harmonic generation. *Physics of Fluids*, *14*(3), 579–590. <https://doi.org/10.1063/1.1693475>
- Matsumoto, H., Kojima, H., Miyake, T., Omura, Y., Okada, M., Nagano, I., & Tsutsui, M. (1994). Electrostatic solitary waves (ESW) in the magnetotail: BEN wave forms observed by GEOTAIL. *Geophysical Research Letters*, *21*, 2915–2918. <https://doi.org/10.1029/94GL01284>
- McFadden, J. P., Carlson, C. W., Ergun, R. E., Mozer, F. S., Muschietti, L., Roth, I., & Moebius, E. (2003). FAST observations of ion solitary waves. *Journal of Geophysical Research*, *108*(A4), 8018. <https://doi.org/10.1029/2002JA009485>
- Mikhailovskii, A. B. (1974). Theory of plasma instabilities: Instabilities of a homogeneous plasma.
- Miyake, T., Omura, Y., Matsumoto, H., & Kojima, H. (1998). Two-dimensional computer simulations of electrostatic solitary waves observed by Geotail spacecraft. *Journal of Geophysical Research*, *103*(A6), 11,841–11,850. <https://doi.org/10.1029/98JA00760>
- Mizuno, K., & Tanaka, S. (1972). Experimental observation of nonlinear wave-particle interactions in a weak cold beam-plasma system. *Physical Review Letters*, *29*(1), 45–48. <https://doi.org/10.1103/PhysRevLett.29.45>
- Morse, R. L., & Nielson, C. W. (1969a). Numerical simulation of warm two-beam plasma. *Physics of Fluids*, *12*, 2418–2425. <https://doi.org/10.1063/1.1692361>
- Morse, R. L., & Nielson, C. W. (1969b). One-, two-, and three-dimensional numerical simulation of two-beam plasmas. *Physical Review Letters*, *23*, 1087–1090. <https://doi.org/10.1103/PhysRevLett.23.1087>
- Mozer, F. S., Agapitov, O. A., Artemyev, A., Burch, J. L., Ergun, R. E., Giles, B. L., et al. (2016). Magnetospheric Multiscale satellite observations of parallel electron acceleration in magnetic field reconnection by Fermi reflection from time domain structures. *Physical Review Letters*, *116*(14), 145,101. <https://doi.org/10.1103/PhysRevLett.116.145101>
- Mozer, F. S., Agapitov, O. V., Artemyev, A., Drake, J. F., Krasnoselskikh, V., Lejosne, S., & Vasko, I. (2015). Time domain structures: What and where they are, what they do, and how they are made. *Geophysical Research Letters*, *42*, 3627–3638. <https://doi.org/10.1002/2015GL063946>
- Mozer, F. S., Agapitov, O. V., Giles, B., & Vasko, I. (2018). Direct observation of electron distributions inside millisecond duration electron holes. *Physical Review Letters*, *121*(13), 135102. <https://doi.org/10.1103/PhysRevLett.121.135102>
- Mozer, F. S., Artemyev, A., Agapitov, O. V., Mourenas, D., & Vasko, I. (2016). Near-relativistic electron acceleration by Landau trapping in time domain structures. *Geophysical Research Letters*, *43*, 508–514. <https://doi.org/10.1002/2015GL067316>
- Mozer, F. S., Ergun, R., Temerin, M., Cattell, C., Dombeck, J., & Wygant, J. (1997). New features of time domain electric-field structures in the auroral acceleration region. *Physical Review Letters*, *79*, 1281–1284. <https://doi.org/10.1103/PhysRevLett.79.1281>
- Muschietti, L., Roth, I., Carlson, C. W., & Ergun, R. E. (2000). Transverse instability of magnetized electron holes. *Physical Review Letters*, *85*, 94–97. <https://doi.org/10.1103/PhysRevLett.85.94>
- Norgren, C., André, M., Graham, D. B., Khotyaintsev, Y. V., & Vaivads, A. (2015). Slow electron holes in multicomponent plasmas. *Geophysical Research Letters*, *42*, 7264–7272. <https://doi.org/10.1002/2015GL065390>
- Norgren, C., André, M., Vaivads, A., & Khotyaintsev, Y. V. (2015). Slow electron phase space holes: Magnetotail observations. *Geophysical Research Letters*, *42*, 1654–1661. <https://doi.org/10.1002/2015GL063218>
- Norgren, C., Hesse, M., Graham, D. B., Khotyaintsev, Y. V., Tenfjord, P., Vaivads, A., et al. (2020). Electron acceleration and thermalization at magnetotail separatrix. *Journal of Geophysical Research: Space Physics*, *125*, e2019JA027440. <https://doi.org/10.1029/2019JA027440>
- Oieroset, M., Sundkvist, D., Chaston, C. C., Phan, T. D., Mozer, F. S., McFadden, J. P., et al. (2014). Observations of plasma waves in the colliding jet region of a magnetic flux rope flanked by two active X lines at the subsolar magnetopause. *Journal of Geophysical Research: Space Physics*, *119*, 6256–6272. <https://doi.org/10.1002/2014JA020124>
- Omura, Y., Matsumoto, H., Miyake, T., & Kojima, H. (1996). Electron beam instabilities as generation mechanism of electrostatic solitary waves in the magnetotail. *Journal of Geophysical Research*, *101*, 2685–2698. <https://doi.org/10.1029/95JA03145>
- Pickett, J., Chen, L., Kahler, S., Santolík, O., Gurnett, D., Tsurutani, B., & Balogh, A. (2004). Isolated electrostatic structures observed throughout the Cluster orbit: Relationship to magnetic field strength. *Annales Geophysicae*, *22*, 2515–2523. <https://doi.org/10.5194/angeo-22-2515-2004>
- Pickett, J. S., Chen, L.-J., Mutel, R. L., Christopher, I. W., Santolík, O., Lakhina, G. S., et al. (2008). Furthering our understanding of electrostatic solitary waves through Cluster multispacecraft observations and theory. *Advances in Space Research*, *41*, 1666–1676. <https://doi.org/10.1016/j.asr.2007.05.064>
- Pollock, C., Moore, T., Jacques, A., Burch, J., Gliese, U., Saito, Y., et al. (2016). Fast plasma investigation for Magnetospheric Multiscale. *Space Science Reviews*, *199*, 331–406. <https://doi.org/10.1007/s11214-016-0245-4>
- Pommois, K., Valentini, F., Pezzi, O., & Veltri, P. (2017). Slow electrostatic fluctuations generated by beam-plasma interaction. *Physics of Plasmas*, *24*(1), 012105. <https://doi.org/10.1063/1.4973829>
- Roberts, K. V., & Berk, H. L. (1967). Nonlinear evolution of a two-stream instability. *Physical Review Letters*, *19*, 297–300. <https://doi.org/10.1103/PhysRevLett.19.297>
- Russell, C. T., Anderson, B. J., Baumjohann, W., Bromund, K. R., Dearborn, D., Fischer, D., et al. (2016). The Magnetospheric Multiscale magnetometers. *Space Science Reviews*, *199*, 189–256. <https://doi.org/10.1007/s11214-014-0057-3>
- Saeki, K., Michelsen, P., Pécseli, H. L., & Rasmussen, J. J. (1979). Formation and coalescence of electron solitary holes. *Physical Review Letters*, *42*, 501–504. <https://doi.org/10.1103/PhysRevLett.42.501>
- Sagdeev, R. Z., & Galeev, A. A. (1969). Nonlinear plasma theory.
- Scarf, F. L., Frank, L. A., Ackerson, K. L., & Lepping, R. P. (1974). Plasma wave turbulence at distant crossings of the plasma sheet boundaries and the neutral sheet. *Geophysical Research Letters*, *1*, 189–192. <https://doi.org/10.1029/GL0011005p00189>
- Schamel, H. (1986). Electron holes, ion holes and double layers. Electrostatic phase space structures in theory and experiment. *Physics Reports*, *140*, 161–191. [https://doi.org/10.1016/0370-1573\(86\)90043-8](https://doi.org/10.1016/0370-1573(86)90043-8)
- Schamel, H. (2000). Hole equilibria in Vlasov-Poisson systems: A challenge to wave theories of ideal plasmas. *Physics of Plasmas*, *7*, 4831–4844. <https://doi.org/10.1063/1.1316767>
- Schmitz, H., Chapman, S. C., & Dendy, R. O. (2002). Electron preacceleration mechanisms in the foot region of high Alfvénic mach number shocks. *The Astrophysical Journal*, *579*(1), 327–336. <https://doi.org/10.1086/341733>
- Steinvaal, K., Khotyaintsev, Y. V., Graham, D. B., Vaivads, A., Le Contel, O., & Russell, C. T. (2019). Observations of electromagnetic electron holes and evidence of Cherenkov whistler emission. *Physical Review Letters*, *123*(25), 255101. <https://doi.org/10.1103/PhysRevLett.123.255101>
- Steinvaal, K., Khotyaintsev, Y. V., Graham, D. B., Vaivads, A., Lindqvist, P. A., Russell, C. T., & Burch, J. L. (2019). Multispacecraft analysis of electron holes. *Geophysical Research Letters*, *46*, 55–63. <https://doi.org/10.1029/2018GL080757>
- Tong, Y., Vasko, I., Mozer, F. S., Bale, S. D., Roth, I., Artemyev, A. V., et al. (2018). Simultaneous multispacecraft probing of electron phase space holes. *Geophysical Research Letters*, *45*, 11,513–11,519. <https://doi.org/10.1029/2018GL079044>

- Tran, M. Q. (1979). Ion acoustic solitons in a plasma: A review of their experimental properties and related theories. *Physica Scripta*, *20*, 317–327. <https://doi.org/10.1088/0031-8949/20/3-4/004>
- Umeda, T., Omura, Y., & Matsumoto, H. (2004). Two-dimensional particle simulation of electromagnetic field signature associated with electrostatic solitary waves. *Journal of Geophysical Research*, *109*, A02207. <https://doi.org/10.1029/2003JA010000>
- Umeda, T., Omura, Y., Miyake, T., Matsumoto, H., & Ashour-Abdalla, M. (2006). Nonlinear evolution of the electron two-stream instability: Two-dimensional particle simulations. *Journal of Geophysical Research*, *111*, A10206. <https://doi.org/10.1029/2006JA011762>
- Vasko, I. Y., Agapitov, O. V., Mozer, F. S., Artemyev, A. V., Drake, J. F., & Kuzichev, I. V. (2017). Electron holes in the outer radiation belt: Characteristics and their role in electron energization. *Journal of Geophysical Research: Space Physics*, *122*, 120–135. <https://doi.org/10.1002/2016JA023083>
- Vasko, I. Y., Agapitov, O. V., Mozer, F., Artemyev, A. V., & Jovanovic, D. (2015). Magnetic field depression within electron holes. *Geophysical Research Letters*, *42*, 2123–2129. <https://doi.org/10.1002/2015GL063370>
- Vasko, I. Y., Agapitov, O. V., Mozer, F. S., Artemyev, A. V., Krasnoselskikh, V. V., & Bonnell, J. W. (2017). Diffusive scattering of electrons by electron holes around injection fronts. *Journal of Geophysical Research: Space Physics*, *122*, 3163–3182. <https://doi.org/10.1002/2016JA023337>
- Vasko, I. Y., Agapitov, O. V., Mozer, F. S., Bonnell, J. W., Artemyev, A. V., Krasnoselskikh, V. V., & Tong, Y. (2018). Electrostatic steepening of whistler waves. *Physical Review Letters*, *120*(19), 195101. <https://doi.org/10.1103/PhysRevLett.120.195101>
- Vasko, I. Y., Krasnoselskikh, V. V., Mozer, F. S., & Artemyev, A. V. (2018). Scattering by the broadband electrostatic turbulence in the space plasma. *Physics of Plasmas*, *25*(7), 072903. <https://doi.org/10.1063/1.5039687>
- Vasko, I. Y., Kuzichev, I. V., Agapitov, O. V., Mozer, F. S., Artemyev, A. V., & Roth, I. (2017). Evolution of electron phase space holes in inhomogeneous plasmas. *Physics of Plasmas*, *24*(6), 062311. <https://doi.org/10.1063/1.4989717>
- Vasko, I. Y., Mozer, F. S., Krasnoselskikh, V. V., Artemyev, A. V., Agapitov, O. V., Bale, S. D., et al. (2018). Solitary waves across supercritical quasi-perpendicular shocks. *Geophysical Research Letters*, *45*, 5809–5817. <https://doi.org/10.1029/2018GL077835>
- Vasko, I. Y., Wang, R., Mozer, F. S., Bale, S. D., & Artemyev, A. V. (2020). On the nature and origin of bipolar electrostatic structures in the Earth's bow shock. *Frontiers in Physics*, *8*, 156. <https://doi.org/10.3389/fphy.2020.00156>
- Viberg, H., Khotyaintsev, Y. V., Vaivads, A., André, M., & Pickett, J. S. (2013). Mapping HF waves in the reconnection diffusion region. *Geophysical Research Letters*, *40*, 1032–1037. <https://doi.org/10.1002/grl.50227>
- Wang, R., Vasko, I. Y., Mozer, F. S., Bale, S. D., Artemyev, A. V., Bonnell, J. W., et al. (2020). Electrostatic turbulence and Debye-scale structures in collisionless shocks. *The Astrophysical Journal*, *889*(1), L9. <https://doi.org/10.3847/2041-8213/ab6582>
- Williams, J. D., Chen, L.-J., Kurth, W. S., Gurnett, D. A., Dougherty, M. K., & Rymer, A. M. (2005). Electrostatic solitary structures associated with the November 10, 2003, interplanetary shock at 8.7 AU. *Geophysical Research Letters*, *32*, L17103. <https://doi.org/10.1029/2005GL023079>
- Wilson, I., Cattell, C. A., Kellogg, P. J., Goetz, K., Kersten, K., Kasper, J. C., et al. (2010). Large-amplitude electrostatic waves observed at a supercritical interplanetary shock. *Journal of Geophysical Research*, *115*, A12104. <https://doi.org/10.1029/2010JA015332>
- Wilson III, L. B., Cattell, C., Kellogg, P. J., Goetz, K., Kersten, K., Hanson, L., et al. (2007). Waves in interplanetary shocks: A Wind/WAVES study. *Physical Review Letters*, *99*(4), 041101. <https://doi.org/10.1103/PhysRevLett.99.041101>
- Wu, M., Lu, Q., Huang, C., & Wang, S. (2010). Transverse instability and perpendicular electric field in two-dimensional electron phase-space holes. *Journal of Geophysical Research*, *115*, A10245. <https://doi.org/10.1029/2009JA015235>
- Zhou, C., & Hutchinson, I. H. (2018). Dynamics of a slow electron hole coupled to an ion-acoustic soliton. *Physics of Plasmas*, *25*(8), 082303. <https://doi.org/10.1063/1.5033859>